symmetry

MDPI

Supplemental Information for

Synchronization in Non-Mirror-Symmetrical Chirogenesis: Non-Helical π–Conjugated Polymers with Helical Polysilane Copolymers in Co-Colloids

Michiya Fujiki [1,*], Shun Okazaki, [1] Nor Azura Abdul Rahim, [1,2,*] Takumi Yamada, [3] and Kotohiro Nomura [3,*]

[1] Graduate School of Science and Technology, Nara Institute of Science and Technology, 8916-5 Takayama, Ikoma, Nara 630-0192, Japan; shunshunshun0508@yahoo.co.jp (S.O.)
[2] Faculty of Chemical Engineering and Technology, Universiti Malaysia Perlis, Kompleks Pusat Pengajian Jejawi 2, Taman Muhibah, Jejawi, 02600 Arau, Perlis, Malaysia
[3] Department of Chemistry, Tokyo Metropolitan University, 1-1 Minami-Osawa, Hachioji, Tokyo 192-0397, Japan; tkm.yamada0714@gmail.com (T.Y.)

* Correspondences: fujikim@ms.naist.jp (M.F.); norazura@unimap.edu.my (N.A.A.R.); ktnomura@tmu.ac.jp (K.T.).

1. Preparation and characterization of samples.

1. Monomer synthesis.

In an analogous previously reported method for *n*-hexyl-(*S*)-2-methylbutylsilanedichloride (**1*S***) and *n*-hexyl-(*R*)-2-methylbutylsilanedichloride (**1*R***) using (*R*)-2-methyl-1-butanol as starting source (100.0 % *ee)*, *n*-hexyl-isobutylsilanedichloride (**2**) using (*S*)-2-methyl-1-butanol as starting source (99.5 % *ee*), and *rac-n*-hexyl-2-methylbutyldichloride (**1*RS***) using (*R*)-2-methyl-1-butanol and (*S*)-2-methyl-1-butanol = 51.17/48.83 (%/%) as starting source were prepared [S1].

1-1. Synthesis of *n*-hexyl-isobutylsilanedichloride (**2**).

A fresh Grignard reagent (i.e., isobutylmagnesium bromide) was prepared from 5.0 g (0.217 mol) of Mg turnings (Wako Chemicals (Osaka, Japan)) and isobutylbromide (Tokyo Chemical Industry (TCI), Tokyo, Japan). First, Mg and 50 mL of dry ether (Kanto Chemicals (Tokyo, Japan)) were placed in a three-neck flask under pure N_2 gas and the Mg surface was activated by adding a few drops of 1,2-dibromoethane (Wako). To this solution, a mixture of 25.0 g (0.18 mol) of isobutylbromide and 80 mL of dry ether was added dropwise for 30 min, and the mixture was maintained at 40 °C for 30 min. A brown coloured solution containing the Grignard reagent was obtained. To a mixture of 51.7 g (0.235 mol)) of *n*-hexyltrichlorosilane (Shin-Etsu Chemical (Tokyo, Japan)) and 50 mL of THF at 55─60 °C in another three-neck flask, the Grignard solution was added dropwise for 2.5 h and maintained at 50 °C for 2 h. The crude monomer was purified by vacuum distillation (bp 80─81 °C/ 2.5 Torr). Yield: 23.2 g (53 %). ^{29}Si-NMR ($CDCl_3$, 25 °C, ppm) 32.644, ^{13}C-NMR ($CDCl_3$, 25 °C, ppm) 32.241, 32.400, 30.485, 25.652 (double intensity), 24.254, 22.550, 22.458, 21.373, 14.123.

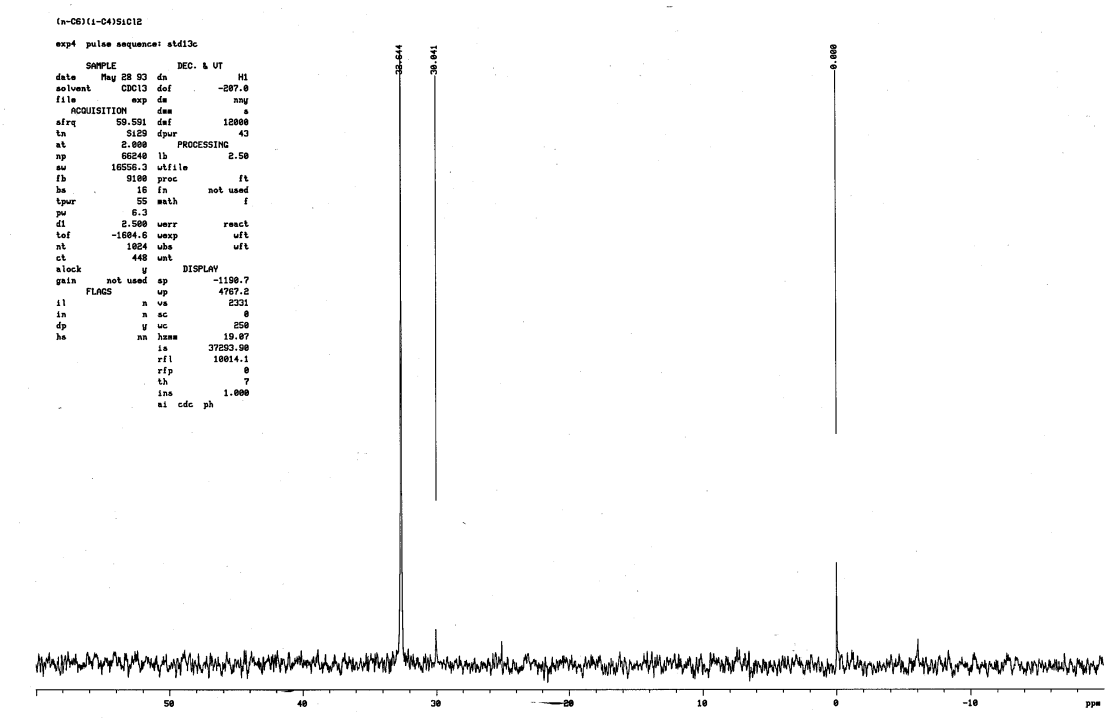

Figure S1. ^{29}Si-NMR spectra of **2** in $CDCl_3$ at 25 °C. ^{29}Si resonances at 32.644 ppm using the Me_4Si ^{29}Si reference peak (0.000 ppm).

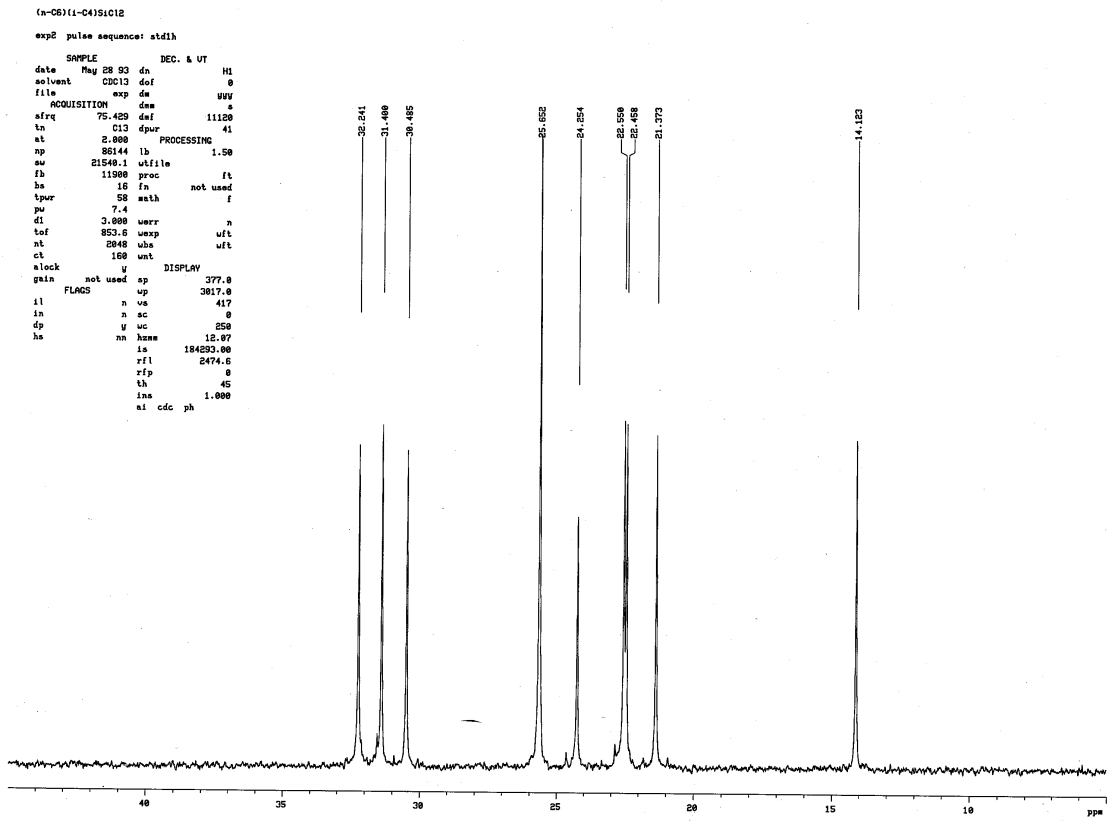

Figure S2. ^{13}C-NMR spectra of **2** in $CDCl_3$ at 25 °C. ^{13}C resonances at 32.241, 32.400, 30.485, 25.652, 24.254, 22.550, 22.458, 21.373, 14.123 ppm vs Me_4Si ^{13}C reference peak (0.000 ppm).

1-2. Synthesis of *n*-hexyl-*rac*-2-methylbutylsilanedichloride (**1*RS***, *R*/*S* = 0.50/0.50).

A fresh Grignard reagent (i.e., *rac*-2-methylbutylmagnesium chloride) was prepared from 11.6 g (0.477 mol) of Mg turnings (Wako Chemicals (Osaka, Japan)) and *rac*-1-chloro-2-methylbutane (Wako, Osaka, Japan). First, Mg and 100 mL of dry THF (Kanto Chemicals (Tokyo, Japan)) were placed in a three-neck flask under pure N_2 gas and the Mg surface was activated by adding a few drops of 1,2-dibromoethane (Wako). To this solution, 42.6 g (0.40 mol) of *rac*-1-chloro-2-methylbutane was added dropwise for 30 min, and the mixture was maintained at 40 °C for 30 min. A coloured solution containing the Grignard reagent was obtained. To a mixture of 226 g (1.03 mol)) of *n*-hexyltrichlorosilane (Shin-Etsu Chemical (Tokyo, Japan)) and 150 mL of THF in another three-neck flask, the Grignard solution was added dropwise for 2 h and maintained at 70 °C for 4 h. The crude monomer was purified by vacuum distillation (bp 120.5—122.0 °C/6.0 Torr). Yield: 57.2 g (53 %). ^{29}Si-NMR ($CDCl_3$, 25 °C, ppm) 33.148, ^{13}C-NMR ($CDCl_3$, 25 °C, ppm) 34.402, 32.206, 31.372, 30.285, 28.150, 22.519, 22.454, 21.862, 21.371, 14.070, 11.227.

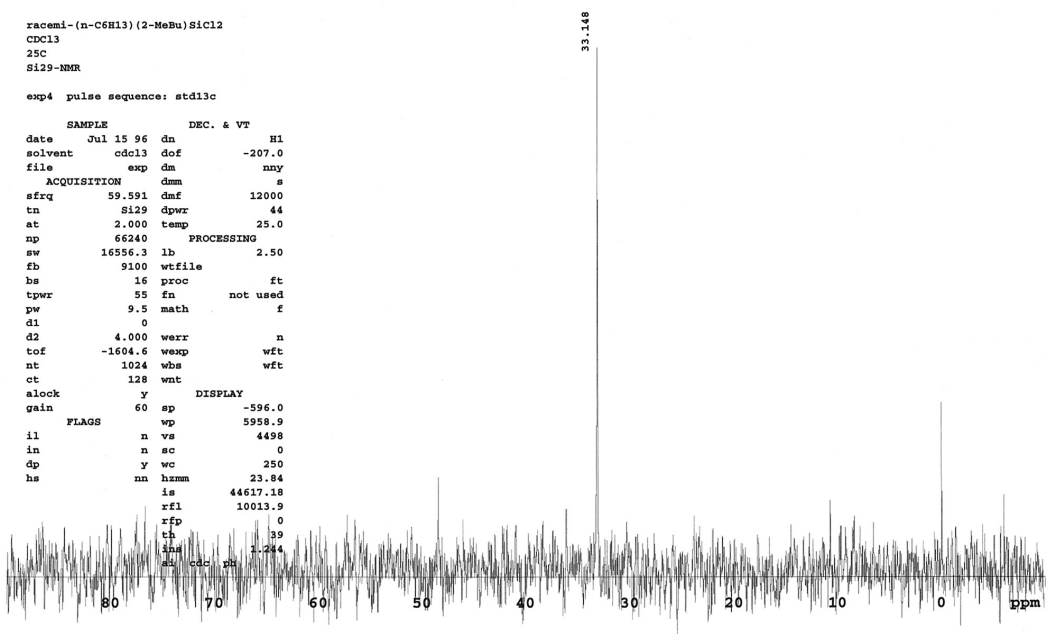

Figure S3. ^{29}Si-NMR spectra of **1-*RS*** in $CDCl_3$ at 30 °C. ^{29}Si resonances at 33.148 ppm using the Me_4Si ^{29}Si reference peak (0.000 ppm).

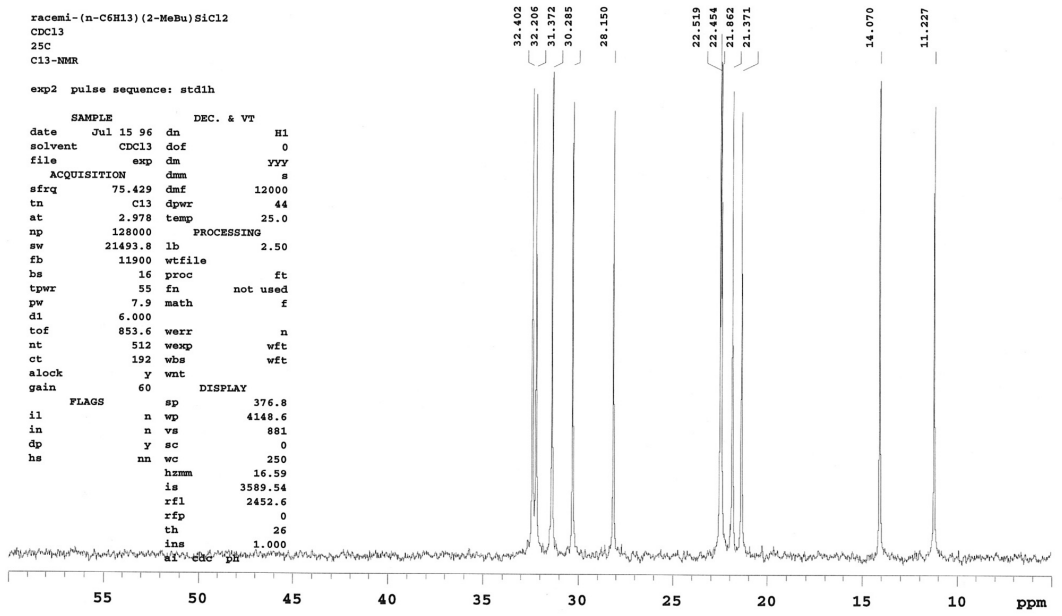

Figure S4. ^{13}C-NMR spectra of **1-*RS*** in $CDCl_3$ at 30 °C. ^{13}C resonances at 34.402, 32.206, 31.372, 30.285, 28.150, 22.519, 22.454, 21.862, 21.371, 14.070, 11.227 ppm vs Me_4Si ^{13}C reference peak (0.000 ppm).

2. Polymer synthesis

*2-1. Synthesis of **HPS-S**, **HPS-R**, **HCPS-SR**, and poly(n-hexyl-isobutylsilane) (**HPS-IB**)*

Rigid rod-like helical **HPS-IB** and **HCPS-*RS*** were prepared according to a previously reported protocol of **HPS-*S*** and **HPS-*R*** [S1].

2-1-1. **HPS-S**. Polymerization of **1*S***

To a mixture containing 50 mL of dry toluene (Wako), 1.0 g (43 mmol) of sodium (Wako), and 0.05 g (0.19 mmol) of 18-crown-6 (Wako) at 120 °C, 5.1 g (20 mmol) of **1*S*** were added dropwise under an N_2 atmosphere. The mixture was slowly stirred at 120 °C for 2 h. The reaction mixture became highly viscous. Additionally, 500 mL of dry toluene was added to reduce the solution viscosity and the resulting mixture was stirred overnight. The hot reaction slurry was passed immediately through Sumitomo Electric Co. (Tokyo, Japan) 40 μm and 2-μm PTFE filter set (Fluoropore F-40 and FP-200, using the pressure of N_2 gas. To the clear filtrate, ethanol and methanol were carefully added. White precipitates were collected by centrifugation with a Kubota (Tokyo, Japan)) model 5420 centrifuge at 3000 rpm followed by drying overnight at 120 °C under vacuum. For the second fraction, ^{29}Si NMR ($CDCl_3$, 30 °C, ppm) exhibited peaks at –22.2, –22.4 and –23.0, and ^{13}C NMR ($CDCl_3$, 30 °C, ppm) exhibited peaks at 34.1, 31.4 and 23.0 [S1].

2-1-2. **HPS-*R***. Polymerization of **1*R***.

Similarly, to a mixture of 25 mL of dry toluene (Wako), 0.80 g (35 mmol) of sodium (Wako) and 0.03 g (0.11 mmol) of 18-crown-6 (Wako) at 120 °C, 2.55 g (10 mmol) of **1*R*** was added dropwise under an N_2 atmosphere. The mixture was stirred at 120 °C for 2 h. The reaction mixture became highly viscous. Additionally, 500 mL of dry toluene were added to reduce the solution viscosity followed by stirring overnight. The hot reaction slurry was passed immediately through the Sumitomo 40-μm and 2-μm PTFE filter set using the pressure of the N_2 gas flow. To the clear filtrate, ethanol and methanol were carefully added. The white precipitates were collected by centrifugation using the Kubota 5420 centrifuge at 3000 rpm and were subsequently died overnight at 120 °C under vacuum. The masses of the first (higher-M_w) and second (middle-M_w) fractions were 0.17 g (9.2 %) and 0.37 g

(20.1 %), respectively. Further fractionations from the second fraction were conducted on the basis of the choice of toluene and poor solvents (IPA, ethanol, methanol and water). Three broad ^{29}Si NMR resonance peaks were observed for the second fraction (100 MHz, $CDCl_3$) at –22.0, –22.2 and –22.7. For the second fraction, the ^{29}Si NMR spectrum ($CDCl_3$, 30 °C, ppm) contained peaks at –22.0, –22.2 and –22.7 [S1].

2-1-3. **HPS-IB**. Polymerization of **2**.

To a mixture containing 50 mL of dry toluene (Wako), 1.0 g (43 mmol) of sodium (Wako), and 0.05 g (0.19 mmol) of 18-crown-6 (Wako) at 120 °C, 2.40 g (10.5 mmol) of **2** were added dropwise under an N_2 atmosphere. The mixture was slowly stirred at 100 °C for 2 h. The reaction mixture became highly viscous. Additionally, 300 mL of dry toluene was added to reduce the solution viscosity and the resulting mixture was stirred overnight. The hot reaction slurry was passed immediately through the Sumitomo 40-μm and 2-μm PTFE filter set under the pressure of N_2 gas. To the clear filtrate, ethanol and methanol were carefully added under gentle stirring. White precipitates were collected by centrifugation with the Kubota 5420 centrifuge at 3000 rpm followed by drying overnight at 120 °C under vacuum. The masses of the first (higher-M_w) and second (middle-M_w) fractions were 0.22 g (12.9 %) and 0.60 g (35.3 %), respectively.

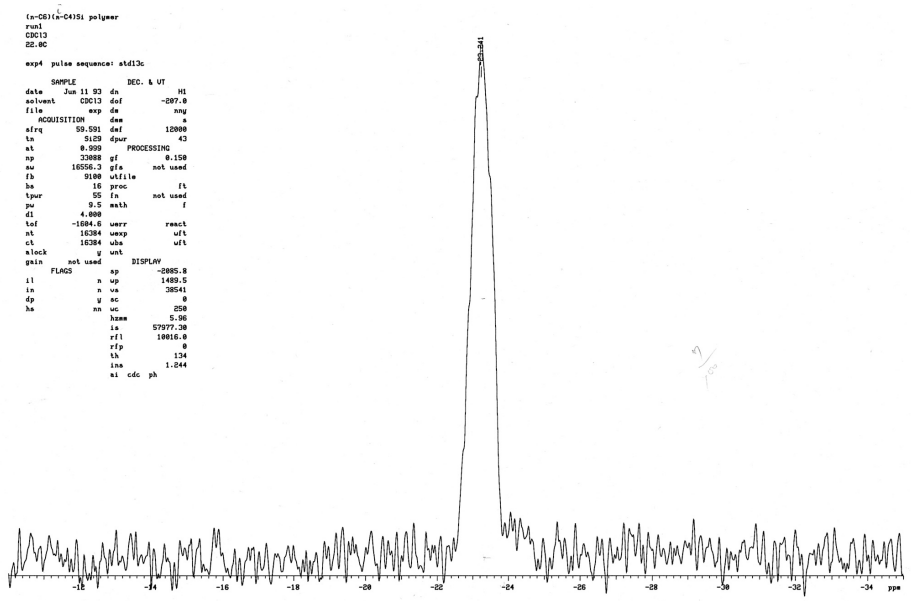

Figure S5. ^{29}Si-NMR spectra of **HPS-IB** in $CDCl_3$ at 25 °C. ^{29}Si resonances at –23.2 ppm using the Me_4Si ^{29}Si reference peak (0.000 ppm).

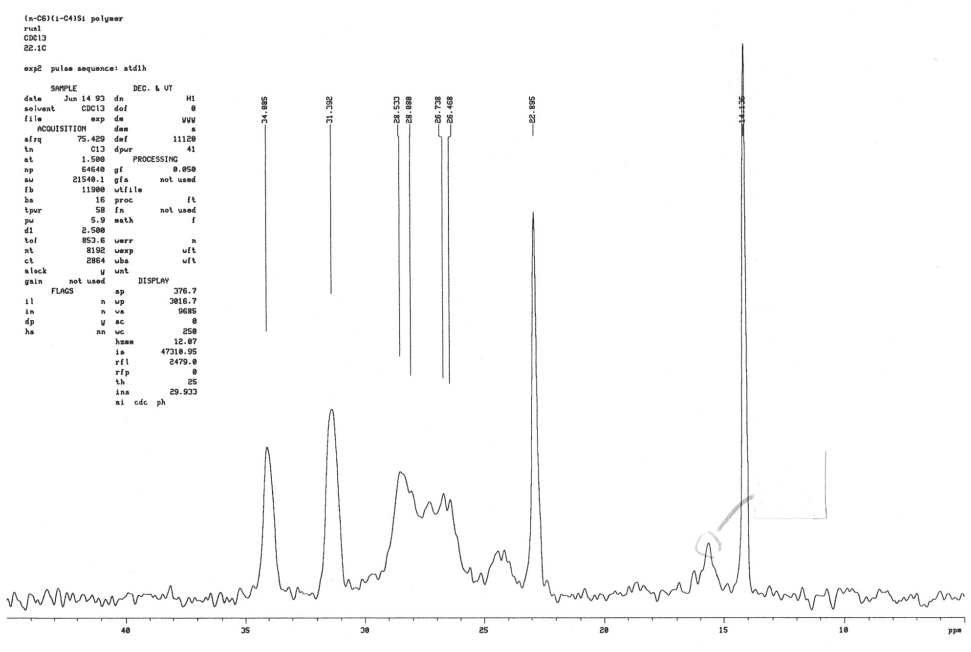

Figure S6. ^{13}C-NMR spectra of **HPS-IB** in $CDCl_3$ at 30 °C. Broad ^{13}C resonances at 34.0, 31.4, 28.5, 28.1, 26.7, 26.5, 24.5, 22.9, 15.5, 14.1 ppm using the Me_4Si ^{29}Si reference peak (0.000 ppm).

Table S1. Molecular weights of **HPS-*S***, **HPS-*R***, **HCPS-*RS*** (*R*/*S* = 0.50/0.50), and **HPS-IB.**

Helical polysilanes	M_n / 10^4	M_w / 10^4	*PDI*	Molecular length / nm
HPS-S	7.58	9.85	1.3	88
HPS-*R*	7.39	11.0	1.5	86
HCPS-*SR*	8.90	23.10	2.6	103
HPS-IB	2.36	5.60	2.4	30

2-1-4. **Type II HCPS-*RS*** (*R*/*S* = 0.50/0.50)**.** Polymerization of **1*RS***.

To a mixture containing 35 mL of dry toluene (Wako), 0.95 g (41 mmol) of sodium (Wako), and 0.055 g (0.21 mmol) of 18-crown-6 (Wako) at 120 °C, 5.1 g (20 mmol) of **1*RS*** were added dropwise under an N_2 atmosphere. The mixture was slowly stirred at 120 °C for 6 h. The reaction mixture became highly viscous. Additionally, 500 mL of dry toluene was added to reduce the solution viscosity and the resulting mixture was stirred overnight. The hot reaction slurry was passed immediately through the Sumitomo 40-μm and 2-μm PTFE filter set using the pressure of N_2 gas. To the clear filtrate, ethanol and methanol were carefully added. White precipitates were collected by centrifugation with the Kubota 5420 centrifuge at 3000 rpm followed by drying overnight at 120 °C under vacuum. The masses of the first (higher-M_w) and second (middle-M_w) fractions were 0.50 g (13.6 %) and 0.74 g (20.1 %), respectively. For the second fraction, ^{29}Si NMR ($CDCl_3$, 25 °C, ppm) exhibited peaks at –22.0, and several broad ^{13}C NMR ($CDCl_3$, 25 °C, ppm) exhibited peaks at 34.0, 31.5, 28.5, 23, 16, 14, 10.5.

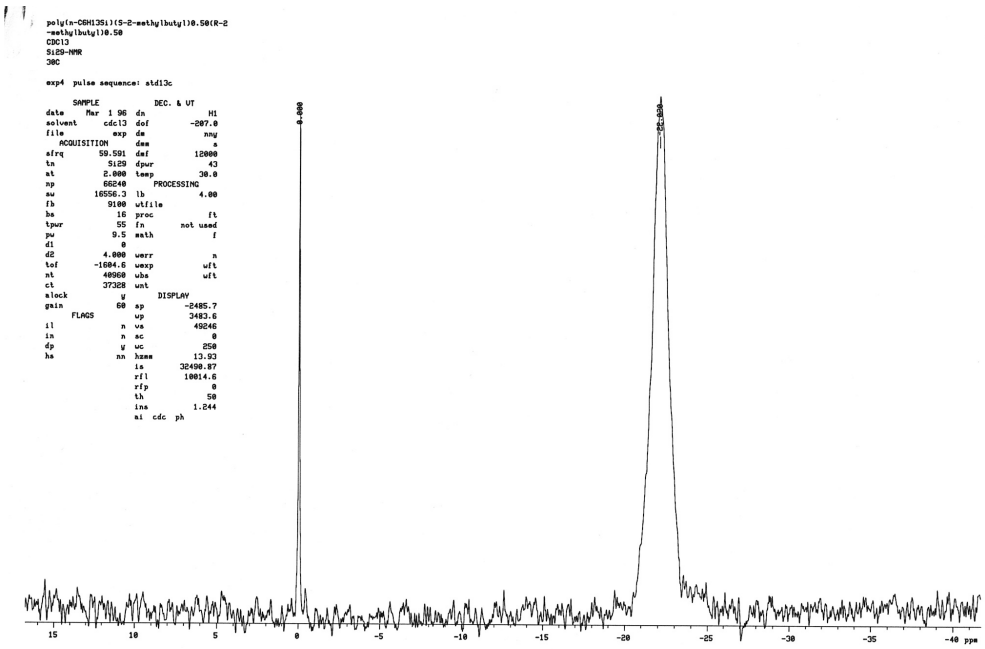

Figure S7. ^{29}Si-NMR spectra of **HCPS-*RS*** (*R*/*S* = 0.50/0.50) in $CDCl_3$ at 25 °C. ^{29}Si resonances at –22.020 ppm using the Me_4Si ^{29}Si reference peak (0.000 ppm).

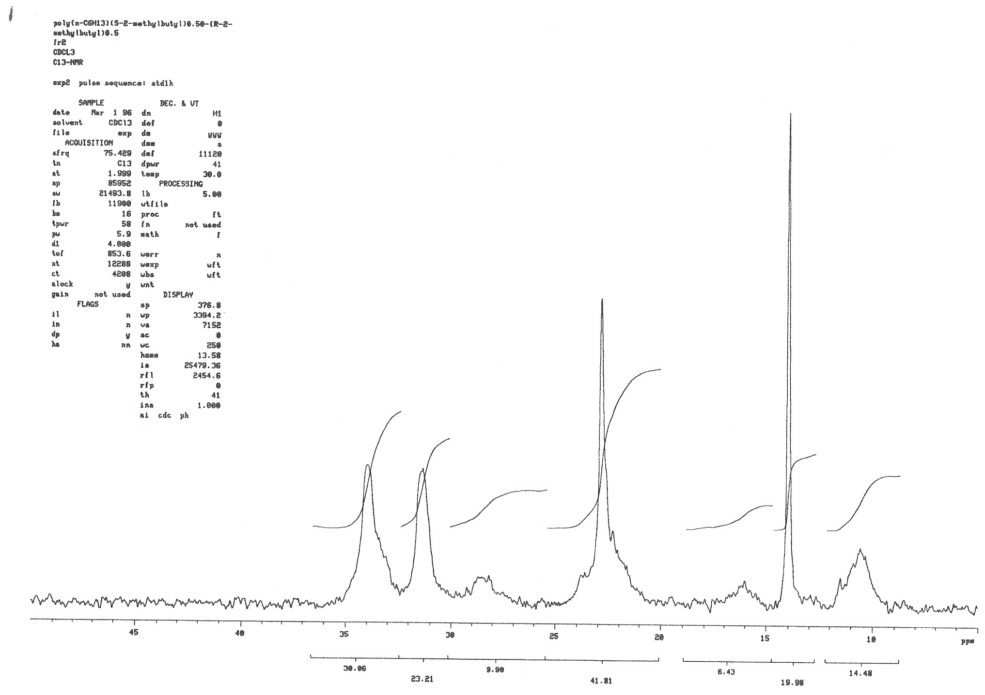

Figure S8. ^{13}C-NMR spectra of **HCPS-*RS*** (*R*/*S* = 0.50/0.50) in $CDCl_3$ at 30 °C. Broad ^{13}C resonances at 34.0, 31.5, 28.5, 23, 16, 14, 10.5 ppm (Me_4Si ^{29}Si reference peak, 0.000 ppm).

2-2. Synthesis of other ***HCPS-S***, ***HCPS-R***, *and* ***HCPS-SR***.

2-2-1. **Type I HCPS-*S*** and **HCPS-*R***. Co-polymerization of **1*S*** with **2** and **1*R*** with **2**.

A representative preparation of **HCPS-*R*** (*R* = 0.10) was outlined as follows. To a mixture containing 20 mL of dry toluene (Wako), 0.70 g (30 mmol) of sodium (Wako), and 0.030 g (0.11 mmol) of 18-crown-6 (Wako) at 120 °C, a mixture of 2.54 g (10.3 mmol) of **1*RS*** and 0.30 g (1.6 mmol) of **1*R*** were added dropwise under an N_2 atmosphere. The mixture was slowly stirred at 120 °C for 6 h. The

reaction mixture became highly viscous. Additionally, 500 mL of dry toluene was added to reduce the solution viscosity and the resulting mixture was stirred overnight. The hot reaction slurry was passed immediately through the Sumitomo 40-μm and 2-μm PTFE filter set using the pressure of N_2 gas. To the clear filtrate, IPA, ethanol, and methanol were carefully added. White precipitates were collected by centrifugation with the Kubota 5420 centrifuge at 3000 rpm followed by drying overnight at 120 °C under vacuum. The masses of the first (higher-M_w) and second (middle-M_w) fractions were 0.06 g (2.9 %) and 0.47 g (23.0 %), respectively.

Other co-polymerizations were carried out using desired mole fractions of **2** with **1*S*** and of **2** with **1*R***. Molecular weight characteristics of **type I HCPS-*S*** and **-*R*** are given in Table S2.

Table S2. Molecular weight characteristics of **type I HCPS** used in this work.

chirality	Mole fraction	M_n /10^4	M_w/ 10^4	*PDI*	Molecular length / nm
(*S*)	0.006	9.55	13.4	1.4	122
(*S*)	0.02	8.00	14.4	1.8	102
(*S*)	0.10	10.78	20.5	1.9	137
(*S*)	0.25	9.60	22.1	2.3	123
(*S*)	0.50	7.15	11.4	1.6	87
(*S*)	1.00	7.58	9.9	1.3	88
(*R*)	0.007	7.88	15.8	2.0	100
(*R*)	0.02	5.78	10.40	1.8	74
(*R*)	0.10	4.77	5.72	1.2	61
(*R*)	0.25	8.52	17.0	2.0	109
(*R*)	0.50	6.56	13.8	2.1	79
(*R*)	1.00	7.39	11.1	1.5	86

*2-2-2. **Type II HCPS-SR**. Co-polymerization of **1S** and **1R**.*

A representative preparation of **HCPS-*SR*** (*S*/*R* = 40/60) was outlined as follows. To a mixture containing 30 mL of dry toluene (Wako), 0.80 g (35 mmol) of sodium (Wako), and 0.030 g (0.11 mmol) of 18-crown-6 (Wako) at 120 °C, a mixture of 2.54 g (9.96 mmol) of **1*RS*** and 0.60 g (2.35 mmol) of **1*R*** were added dropwise under an N_2 atmosphere. The mixture was slowly stirred at 120 °C for 14 h. The reaction mixture became highly viscous. Additionally, 500 mL of dry toluene was added to reduce the solution viscosity and the resulting mixture was stirred overnight. The hot reaction slurry was passed immediately through the Sumitomo 40-μm and 2-μm PTFE filter set using the pressure of N_2 gas. To the clear filtrate, IPA, ethanol, and methanol were carefully added. White precipitates were collected by centrifugation with the Kubota 5420 centrifuge at 3000 rpm followed by drying overnight at 120 °C under vacuum. The masses of the first (higher-M_w) and second (middle-M_w) fractions were 0.03 g (1.3 %) and 0.26 g (11.5 %), respectively.

Other co-polymerizations were employed using desired mole fractions of **1*RS*** with **1*S*** and of **1*RS*** with **1*R***. Molecular weight characteristics of **type II HCPS-*SR*** are given in Table S3.

Table S3. Molecular weight characteristics of **type II HCPS-*SR*** used in this work.

mole fraction chirality		M_n /10^4	M_w/ 10^4	*PDI*	Molecular length / nm
(*S*)/(*R*)	1.00/0.00	7.58	9.9	1.3	88
(*S*)/(*R*)	0.60/0.40	7.45	18.63	2.5	87
(*S*)/(*R*)	0.53/0.47	4.55	9.10	2.0	52
(*S*)/(*R*)	0.50/0.50	8.90	23.10	2.6	103
(*S*)/(*R*)	0.47/0.53	5.78	10.40	1.8	67
(*S*)/(*R*)	0.40/0.60	4.88	9.76	2.0	56
(*S*)/(*R*)	0.00/1.00	7.39	11.10	1.5	86

2-3. Main chain rigidity of ***HPS-S***, ***HPS-R***, *and* ***HPS-IB***.

The degree of polysilane stiffness was confirmed by the high viscosity index observed in the viscometric data (α) in the Kuhn-Mark-Houwink-Sakurada plots ($[\eta] = \kappa \cdot M^{\alpha}$, where $[\eta]$ is the intrinsic viscosity, M is the molecular mass, κ is a constant, and α is the viscosity index) in toluene at 70 °C. The viscometric measurement has been well established as a physico-chemical method for the characterisation of floppy chain-like polymers in dilute solution. The α values of **HPS-*S***, **HPS-*R***, and **HPS-IB** in toluene at 70 °C were 1.24, 1.76, and 1.62, respectively. Three **HPS-*S***, **HPS-*R***, and **HPS-IB** adopt rod-like conformations in dilute toluene solutions. Similarly, other polysilane homopolymers and copolymers revealed higher viscosity indices (Figure 10, main text), indicating an adoption of rod-like conformations in dilute toluene at 70 °C. Possibly, these helical polysilanes should adopt rod-like conformations in dilute chloroform and toluene solutions even at room temperature.

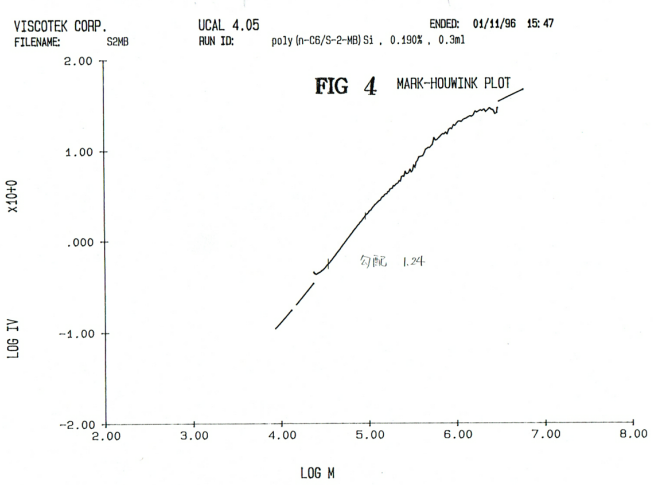

Figure S9. Raw data of log[η] as a function of log$M$ for **HPS-*S*** in toluene at 70 °C. The TRC (file no. TRC-T11433/111093) with NTT R&D center measured and analysed the samples. The Figure was taken from Electronic Supporting Information (ESI) of ref [67].

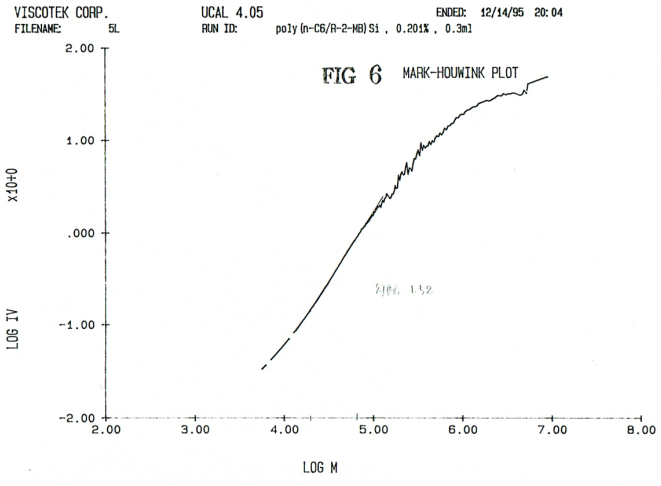

Figure S10. Raw data of log[η] as a function of log$M$ for **HPS-*R*** in toluene at 70 °C. The TRC (file no. TRC-T11433/T111093) with NTT R&D center measured and analysed the samples. The Figure was taken from ESI of ref [67].

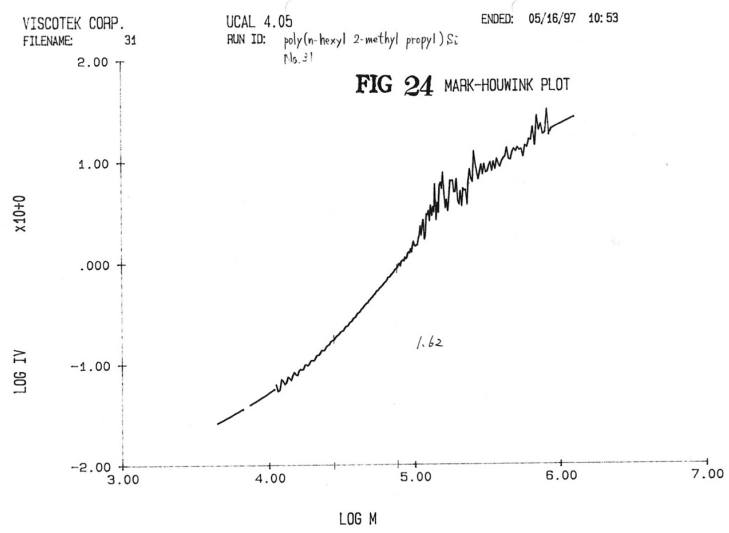

Figure S11. Raw data of log[η] as a function of log$M$ for poly(*n*-hexyl-isobutylsilane) (**HPS-IB**) in toluene at 70 °C. Toray Research Company (TRC: file no. TRC-T114352) with NTT R&D center measured and analysed the samples.

2-4. Main chain rigidity of ***type I HCPS-S*** *and* ***type I HCPS-R****.*

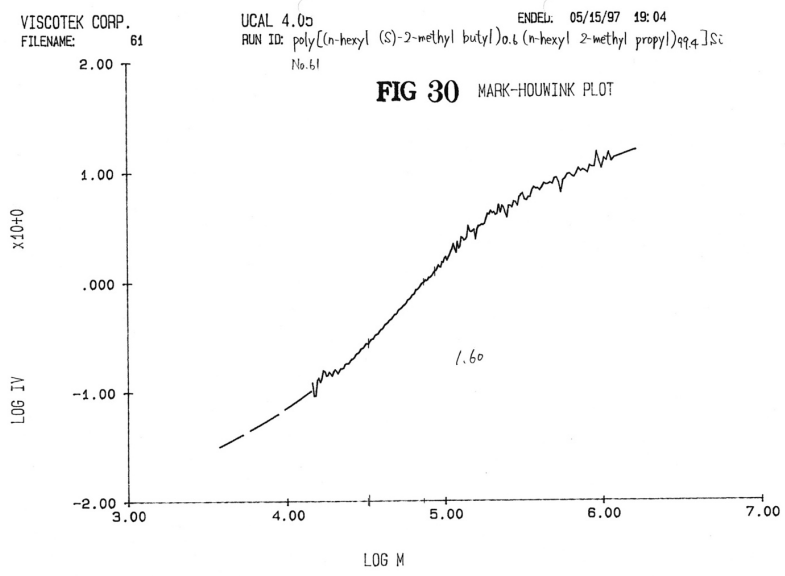

Figure S12. Raw data of log[η] as a function of log$M$ for **Type I HCPS, (1S)$_{0.006}$–(2)$_{0.994}$,** in toluene at 70 °C. TRC (file no. TRC-T114352) with NTT R&D center measured and analysed the samples.

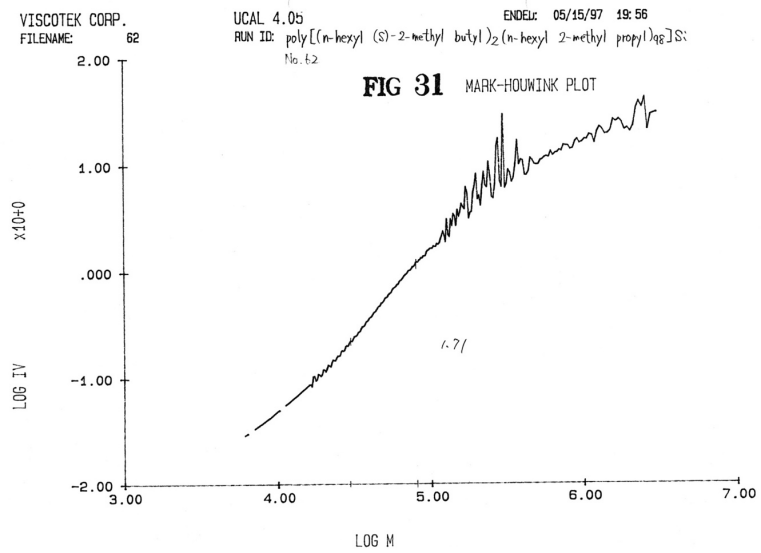

Figure S13. Raw data of log[η] as a function of log$M$ for **Type I HCPS, (1S)$_{0.02}$–(2)$_{0.98}$**, in toluene at 70 °C. TRC (file no. TRC-T114352) with NTT R&D center measured and analysed the samples.

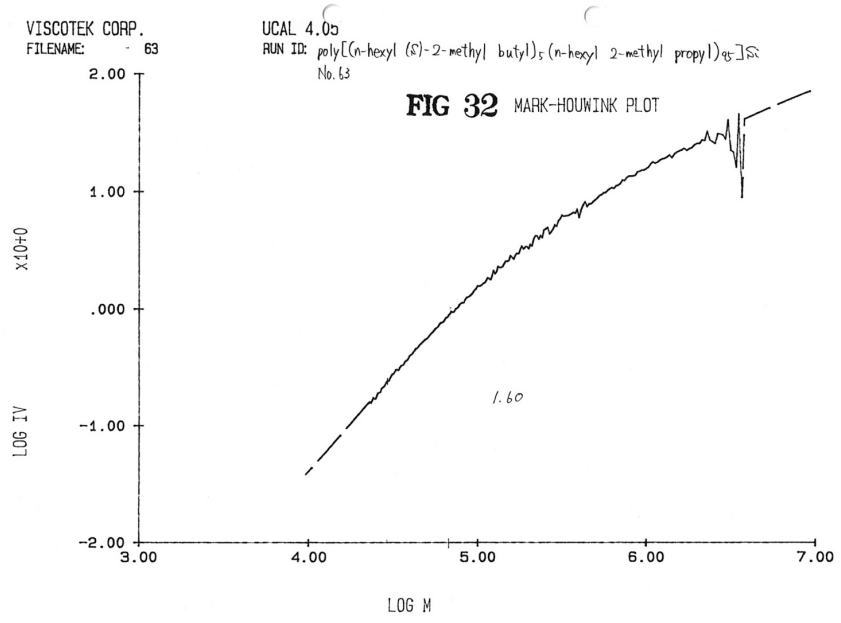

Figure S14. Raw data of log[η] as a function of log$M$ for **Type I HCPS, (1S)$_{0.05}$–(2)$_{0.95}$**, in toluene at 70 °C. TRC (file no. TRC-T114352) with NTT R&D center measured and analysed the samples.

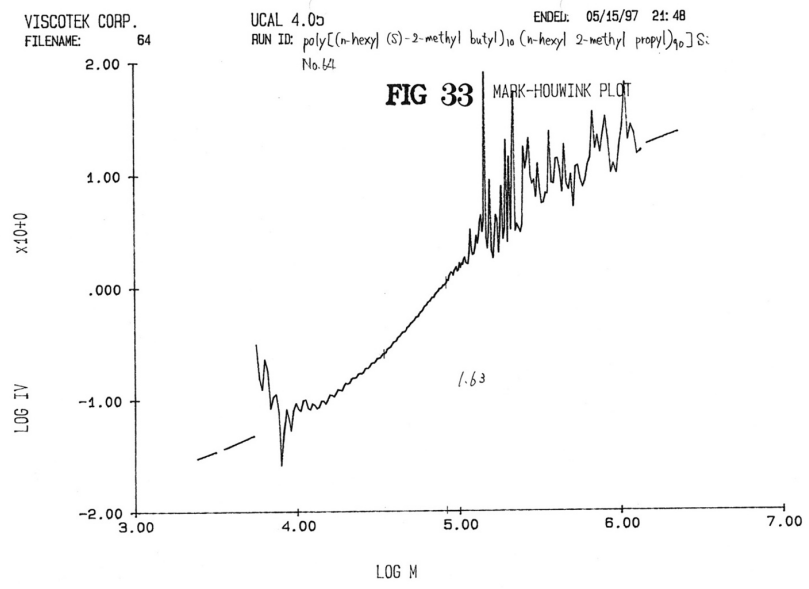

Figure S15. Raw data of log[η] as a function of log$M$ for **Type I HCPS, (1*S*)$_{0.10}$–(2)$_{0.90}$,** in toluene at 70 °C. TRC (file no. TRC-T114352) with NTT R&D center measured and analysed the samples.

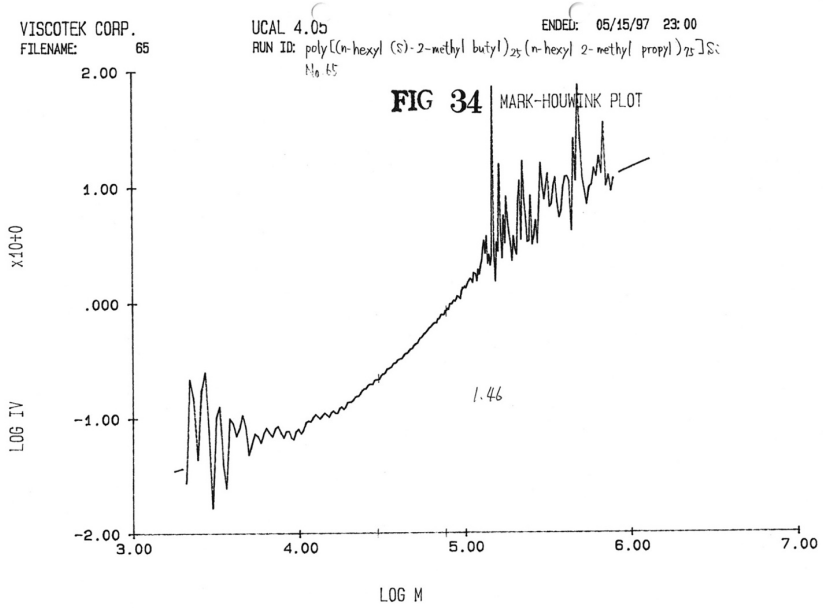

Figure S16. Raw data of log[η] as a function of log$M$ for **Type I HCPS, (1*S*)$_{0.25}$–(2)$_{0.75}$,** in toluene at 70 °C. TRC (file no. TRC-T114352) with NTT R&D center measured and analysed the samples.

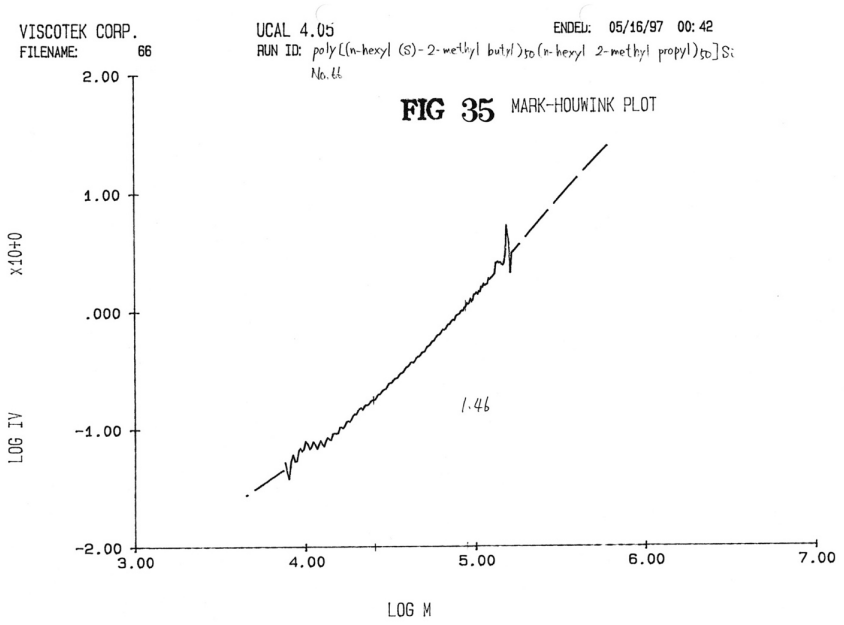

Figure S17. Raw data of log[η] as a function of log$M$ for **Type I HCPS, (1*S*)$_{0.50}$–(2)$_{0.50}$,** in toluene at 70 °C. TRC (file no. TRC-T114352) with NTT R&D center measured and analysed the samples.

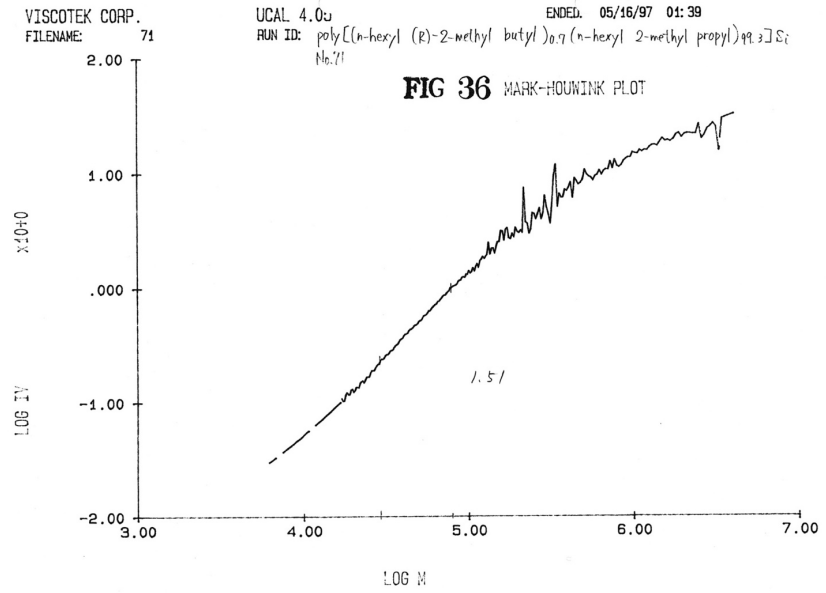

Figure S18. Raw data of log[η] as a function of log$M$ for **Type I HCPS, (1*R*)$_{0.007}$–(2)$_{0.993}$,** in toluene at 70 °C. TRC (file no. TRC-T114352) with NTT R&D center measured and analysed the samples.

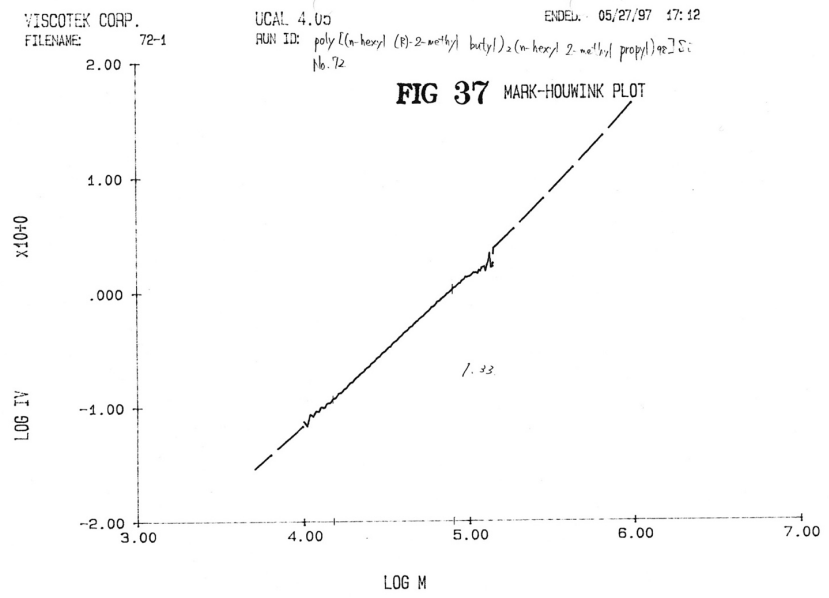

Figure S19. Raw data of log[η] as a function of log$M$ for **Type I HCPS, (1*R*)$_{0.02}$-(2)$_{0.98}$,** in toluene at 70 °C. TRC (file no. TRC-T114352) with NTT R&D center measured and analysed the samples.

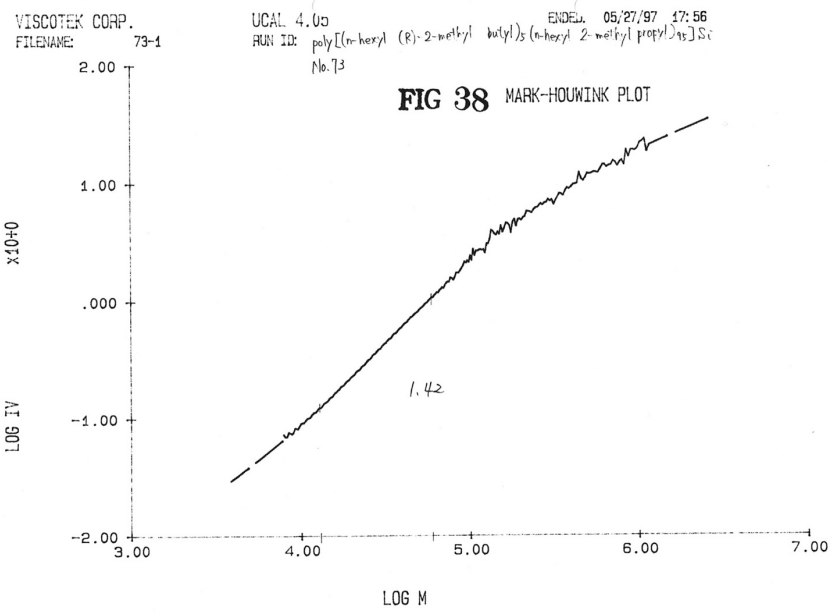

Figure S20. Raw data of log[η] as a function of log$M$ for **Type I HCPS, (1*R*)$_{0.05}$-(2)$_{0.95}$,** in toluene at 70 °C. TRC (file no. TRC-T114352) with NTT R&D center measured and analysed the samples.

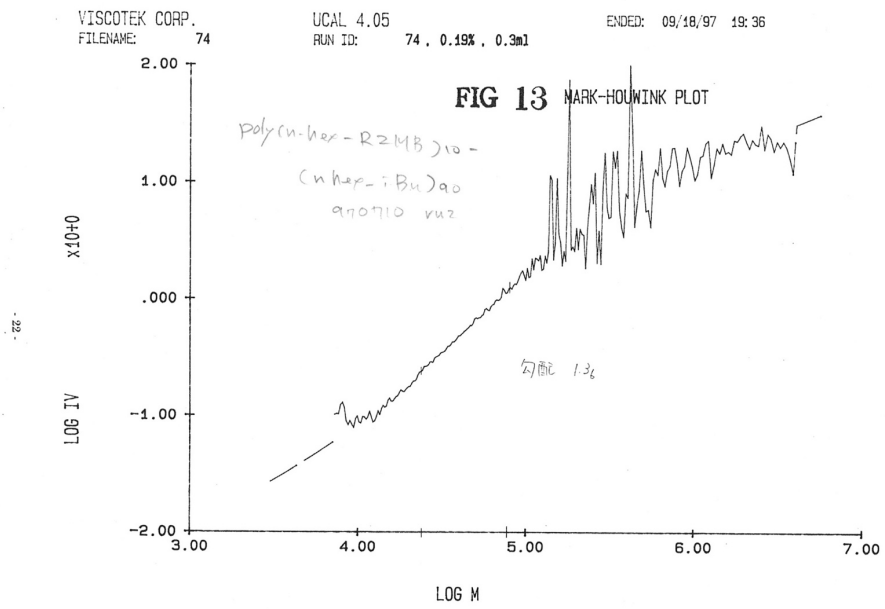

Figure S21 Raw data of log[η] as a function of log$M$ for **Type I HCPS, (1*R*)$_{0.10}$-(2)$_{0.90}$,** in toluene at 70 °C. TRC (file no. TRC-T215754) with NTT R&D center measured and analysed the samples.

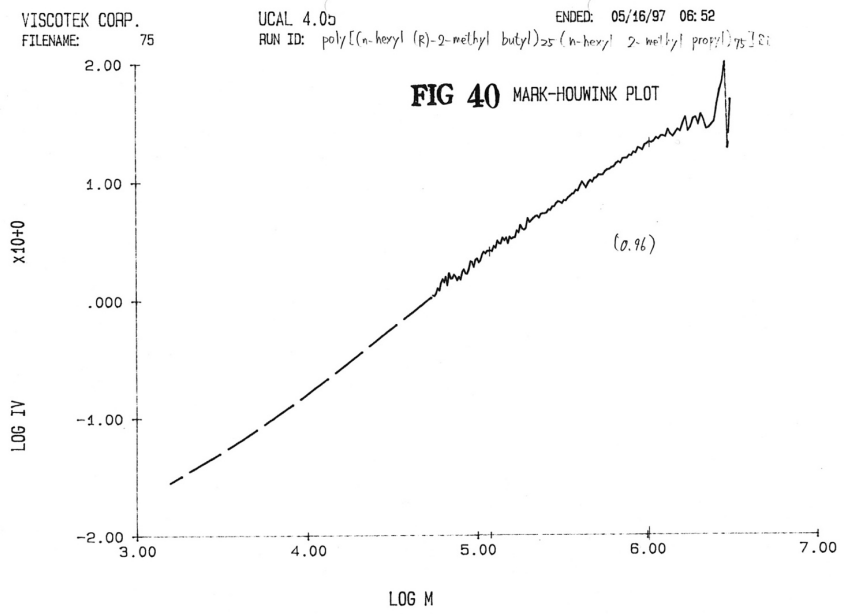

Figure S22. Raw data of log[η] as a function of log$M$ for **Type I HCPS, (1*R*)$_{0.25}$-(2)$_{0.75}$,** in toluene at 70 °C. TRC (file no. TRC-T114352) with NTT R&D center measured and analysed the samples.

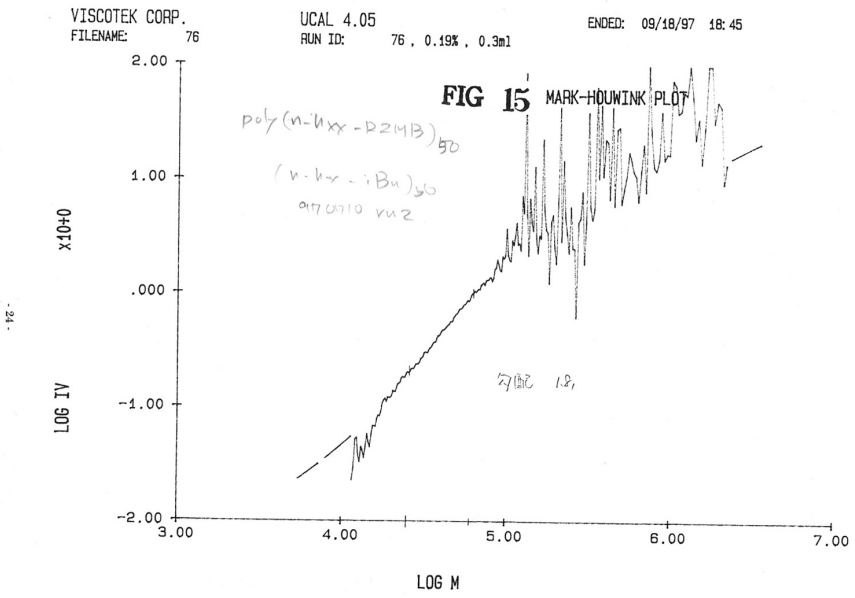

Figure S23. Raw data of log[η] as a function of log$M$ for **Type I HCPS, (1*R*)$_{0.50}$-(2)$_{0.50}$,** in toluene at 70 °C. TRC (file no. TRC-T114352 and TRC-T215754) with NTT R&D center measured and analysed the samples.

2-6. Main chain rigidity of ***type II HCPS-SR***.

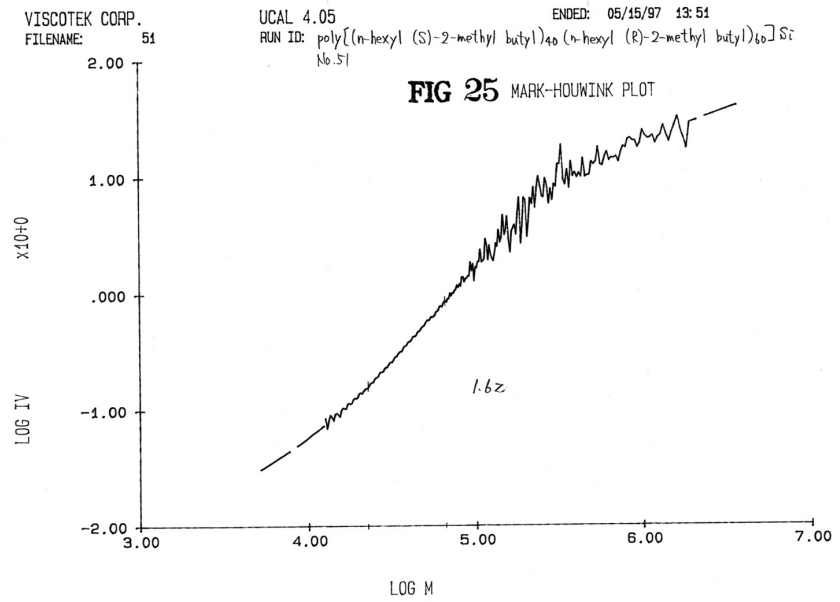

Figure S24. Raw data of log[η] as a function of log$M$ for **Type II HCPS, (1*S*)$_{0.40}$–(1*R*)$_{0.60}$,** in toluene at 70 °C. TRC (file no. TRC-T114352) with NTT R&D center measured and analysed the samples.

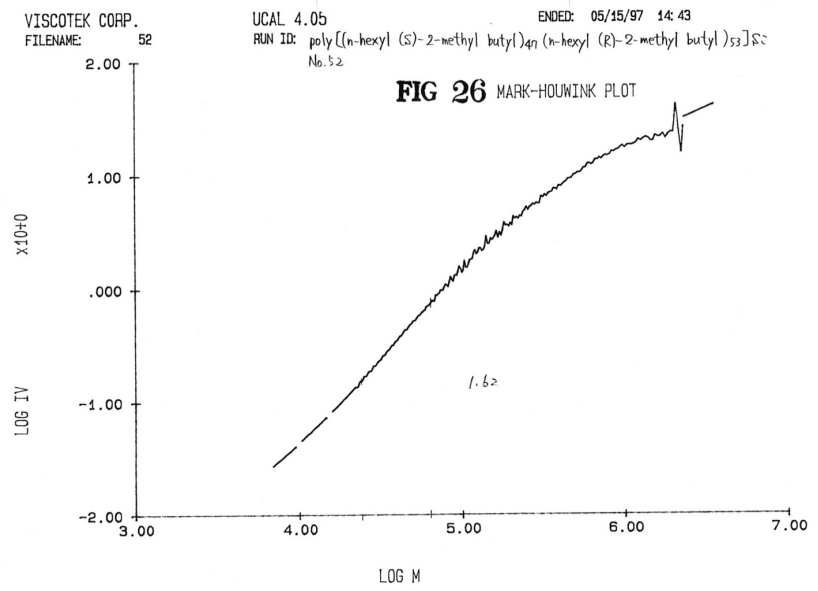

Figure S25. Raw data of log[η] as a function of log$M$ for **Type II HCPS, (1*S*)$_{0.47}$–(1*R*)$_{0.53}$,** in toluene at 70 °C. TRC (file no. TRC-T114352) with NTT R&D center measured and analysed the samples.

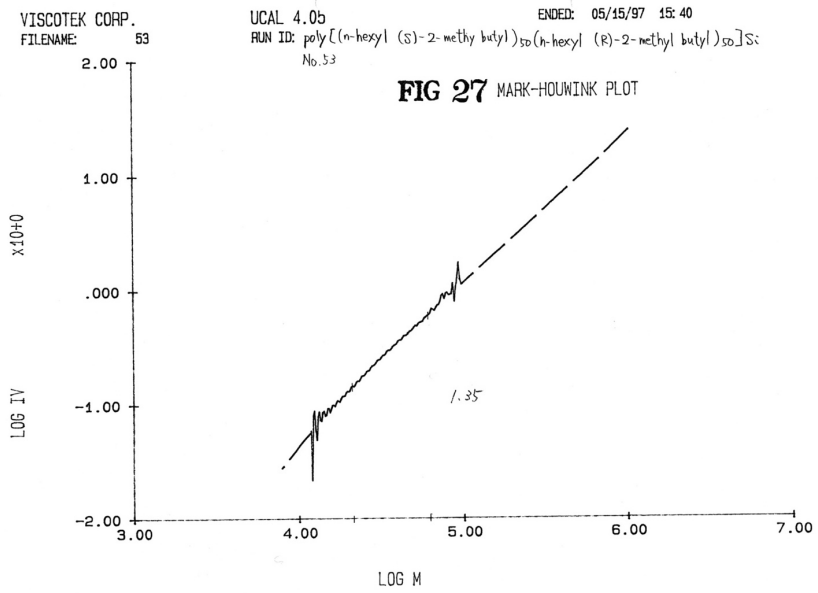

Figure S26. Raw data of log[η] as a function of log$M$ for **Type II HCPS, (1*S*)$_{0.50}$–(1*R*)$_{0.50}$,** in toluene at 70 °C. TRC (file no. TRC-T114352) with NTT R&D center measured and analysed the samples.

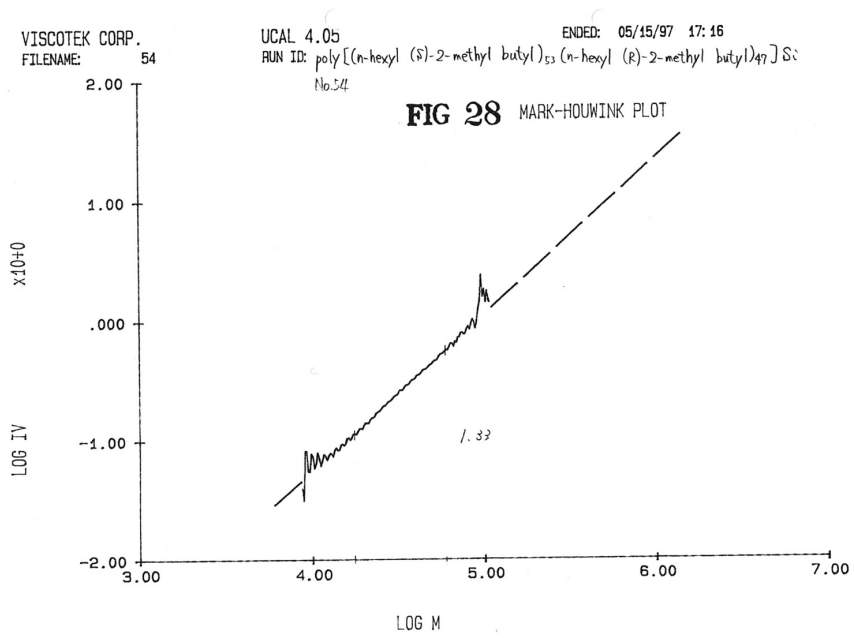

Figure S27. Raw data of log[η] as a function of log$M$ for **Type II HCPS, (1*S*)$_{0.53}$–(1*R*)$_{0.47}$,** in toluene at 70 °C. TRC (file no. TRC-T114352) with NTT R&D center measured and analysed the samples.

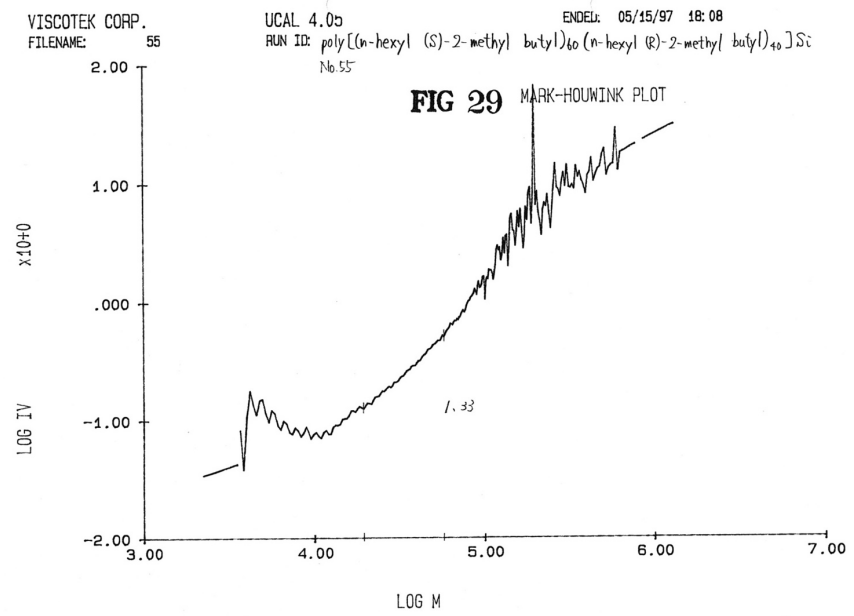

Figure S28. Raw data of log[η] as a function of log$M$ for **Type II HCPS, (1*S*)$_{0.60}$–(1*R*)$_{0.40}$,** in toluene at 70 °C. TRC (file no. TRC-T114352) with NTT R&D center measured and analysed the samples.

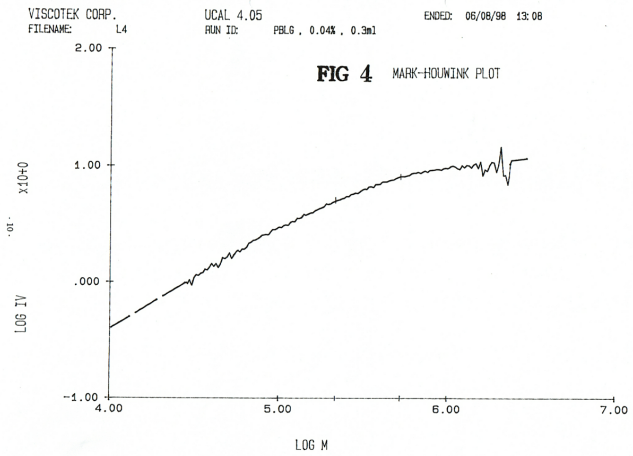

Figure S29. Raw data of log[η] as a function of log$M$ for helical poly-γ-benzyl-*L*-glutamate (PBLG, purchased from Sigma-Aldrich) in DMF with 0.05 M LiCl at 30 °C. TRC (file no. TRC-T217253) with NTT R&D center measured and analysed the samples.

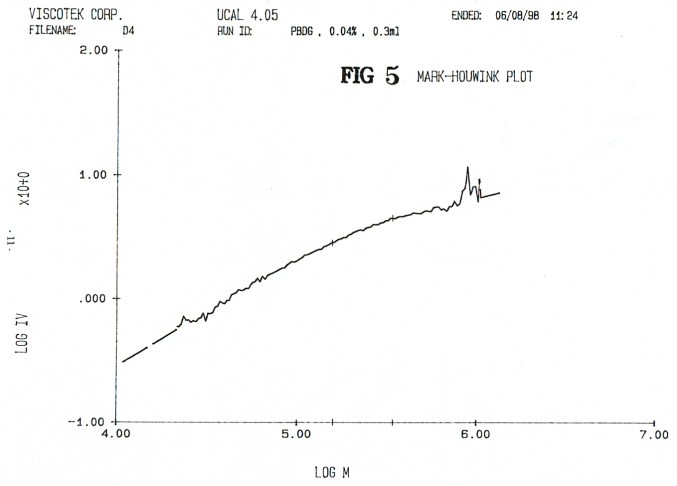

Figure S30. Raw data of log[η] as a function of log$M$ for helical poly-γ-benzyl-*D*-glutamate (PBDG, purchased from Sigma-Aldrich) in DMF with 0.05 M LiCl at 30 °C. TRC (file no. TRC-T217253) with NTT R&D center measured and analysed the samples.

ＧＰＣ－ＶＩＳＣＯ(ゲル浸透クロマトグラフー粘度検出器、0.05N-LiCl添加DMF、３０℃)法により、ＰＢＬＧおよびＰＢＤＧの極限粘度測定を行った。極限粘度－分子量の指数の結果を次表に示す。指数の値は測定試料が有する分子量範囲に限られていることを考慮されたい。

試料	極限粘度－分子量の指数
ＰＢＬＧ	０.５４
ＰＢＤＧ	０.５６

なお、両試料の粘度式は次のとおりである。

$$\text{PBLG}: [\eta] = 6.6_5 \times 10^{-3} M^{0.54}$$
$$\text{PBDG}: [\eta] = 3.5_7 \times 10^{-3} M^{0.56}$$

Figure S31. Report (in Japanese) of viscometric parameters between PBLG and PBDG. TRC (file no. TRC-T217253) with NTT R&D center measured and analysed the samples.

*2-7. Fractionation of **PFV8** and **PF8*** used in this work.

PFV8 used in this work was fractionated to two (high/low molecular weight) fractions using *n*-hexane [S2]. The values of M_n, M_w, and *PDI* were 2.47 x 10^4, 3.27 x 10^4, and 1.32, respectively. The main chain lengths of **PFV8** were evaluated to be 6.2 nm by the product of the monomer unit length (1.05 nm) and number-average degree of polymerization $DP_n = M_n/M_0$, where M_n and M_0 are the number-average of molecular weight and the molecular weight of the monomer unit.

Also, a broad molecular weight dispersity **PF8** (*PDI* = 3.6) purchased from Sigma-Aldrich Japan (Tokyo, Japan, now Merck group) was fractionated by adding a poor solvent to a chloroform solution of **PF8**. In the fractionation process, **PF8** was dissolved in chloroform (Wako, special grade), followed by the gradual addition of isopropanol (IPA) during gentle stirring until the colloid was generated in the stock solution. The polymer was filtered with a PTFE 1.0 μm membrane filter. The remaining **PF8** on the filter was collected and dried in a vacuum oven overnight. Similar fractionation processes were repeated with higher-polarity solvents (i.e., ethanol and methanol). A narrower *PDI* with higher M_n and M_w sample of **PF8** (M_n = 78,400, M_w = 141,100, *PDI* = 1.80) was chosen for this study. The main chain lengths of **PF8** was evaluated to be 16.9 nm by the product of the monomer unit length (0.84 nm) and $DP_n = M_n/M_0$.

Table S4. Molecular weight characteristics of **PFV8** and **PF8** used in this work.

Helical polysilanes	M_n / 10^4	M_w / 10^4	*PDI*	Molecular length / nm
PFV8	2.47	3.27	1.32	6.2
PF8	7.84	14.1	1.80	16.9

3. Dynamic light scattering analysis of co-colloidal ***PFV8*** *with* ***HPS-S***, ***PFV8*** *with* ***HPS-R***, and ***PFV8*** *with* ***HCPS-SR*** [(*S*)/(*R*) = *0.50/0.50)*].

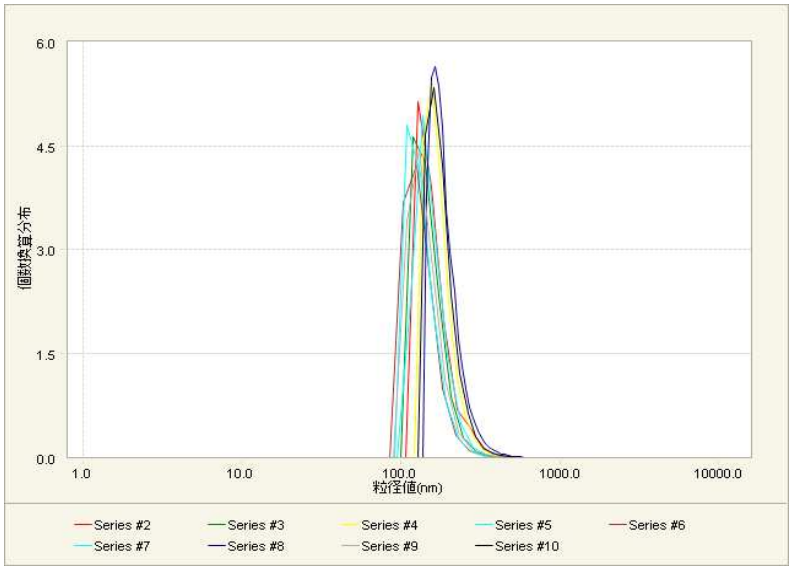

No.	DataName	Color	Diameter(nm)	Cumu.(10%)(nm)	Cumu.(50%)(nm)	Cumu.(90%)(nm)
1	20180118PFV-PSi-	Blue	513.2	119.9	254.6	340.2
2	20180118PFV-PSi-S_	Red	305.1	112.1	135.7	191.6
3	20180118PFV-PSi-S_	Green	288.2	104.4	128.0	174.2
4	20180118PFV-PSi-S_	Yellow	306.4	127.1	152.5	206.7
5	20180118PFV-PSi-S_	Cyan	292.1	105.6	132.9	185.1
6	20180118PFV-PSi-S_	Brown	287.9	90.6	114.5	160.1
7	20180118PFV-PSi-S_	Aqua	279.3	95.5	116.8	159.1
8	20180118PFV-PSi-S_	DarkBlue	321.3	146.6	173.3	238.9
9	20180118PFV-PSi-S_	DarkGray	294.9	96.5	122.0	170.2
10	20180118PFV-PSi-S_	Black	318.2	133.9	160.6	217.9

Figure S32. Changes in particle size of **PFV8-HPS-*S*** co-colloids in $CHCl_3$/MeOH = 2.0/1.0 (v/v) before the 313-nm UV irradiation.

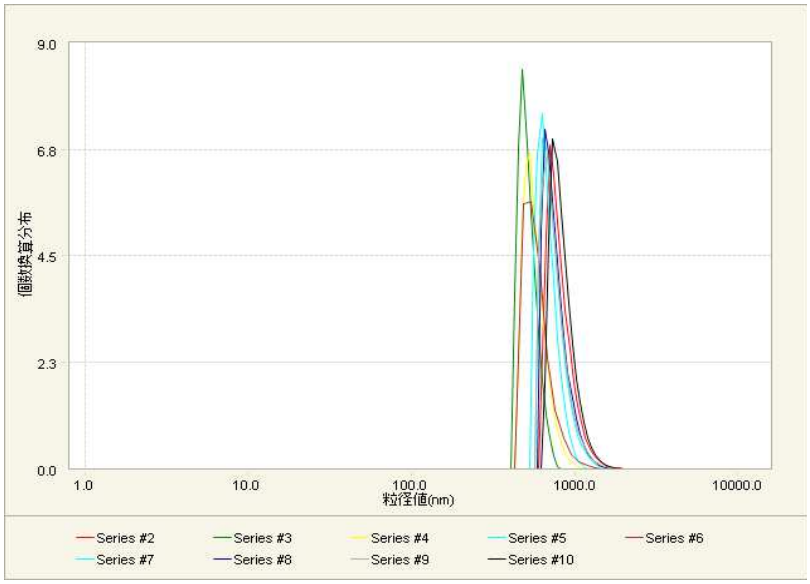

No.	DataName	Color	Diameter(nm)	Cumu.(10%)(nm)	Cumu.(50%)(nm)	Cumu.(90%)(nm)
1	20180118PFV-PSi-	Blue	513.2	119.9	254.6	340.2
2	20180118PFV-PSi-	Red	1118.1	647.0	752.6	991.8
3	20180118PFV-PSi-	Green	645.9	433.3	489.7	596.5
4	20180118PFV-PSi-	Yellow	727	461.9	535.7	687.7
5	20180118PFV-PSi-	Cyan	897.8	560.3	640.6	800.1
6	20180118PFV-PSi-	Brown	879.6	450.8	530.9	709.5
7	20180118PFV-PSi-	Aqua	1020.8	601.8	692.7	905.4
8	20180118PFV-PSi-	DarkBlue	1030	620.0	712.6	928.9
9	20180118PFV-PSi-	DarkGray	1079.1	603.0	700.7	925.4
10	20180118PFV-PSi-	Black	1157.7	679.9	787.2	1023.9

Figure S33. Changes in particle size of **PFV8-HPS-*S*** co-colloids in $CHCl_3$/MeOH = 2.0/1.0 (v/v) after the 313-nm UV irradiation (20 μW cm^{-2}) for 10 sec.

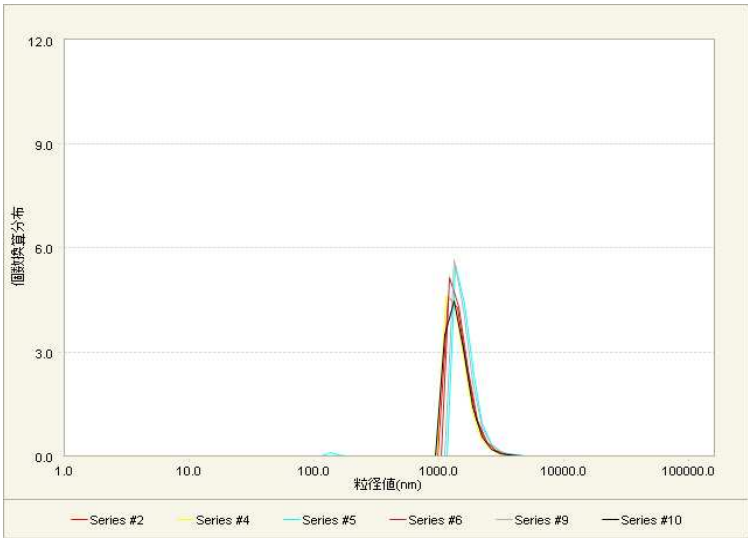

No.	DataName	Color	Diameter(nm)	Cumu.(10%)(nm)	Cumu.(50%)(nm)	Cumu.(90%)(nm)
1	20180117PFV-PSi-R_	Blue	3168.9	83.1	90.2	1692.0
2	20180117PFV-PSi-R_	Red	4277.1	1042.2	1280.7	1787.6
3	20180117PFV-PSi-R_	Green	2924.1	1833.6	2056.8	2480.0
4	20180117PFV-PSi-R_	Yellow	3270.7	1016.5	1244.2	1724.8
5	20180117PFV-PSi-R_	Cyan	3450.1	1199.8	1430.9	1945.4
6	20180117PFV-PSi-R_	Brown	3546.3	1088.2	1315.0	1819.2
7	20180117PFV-PSi-R_	Aqua	3704.3	1098.9	1314.3	1794.5
8	20180117PFV-PSi-R_	DarkBlue	3857.3	156.1	1509.3	2059.4
9	20180117PFV-PSi-R_	DarkGray	4035	1154.5	1372.2	1857.3
10	20180117PFV-PSi-R_	Black	4034.8	1009.6	1270.1	1782.2

Figure S34. Changes in particle size of **PFV8-HPS-*R*** co-colloids in $CHCl_3$/MeOH = 2.0/1.0 (v/v) before the 313-nm UV irradiation.

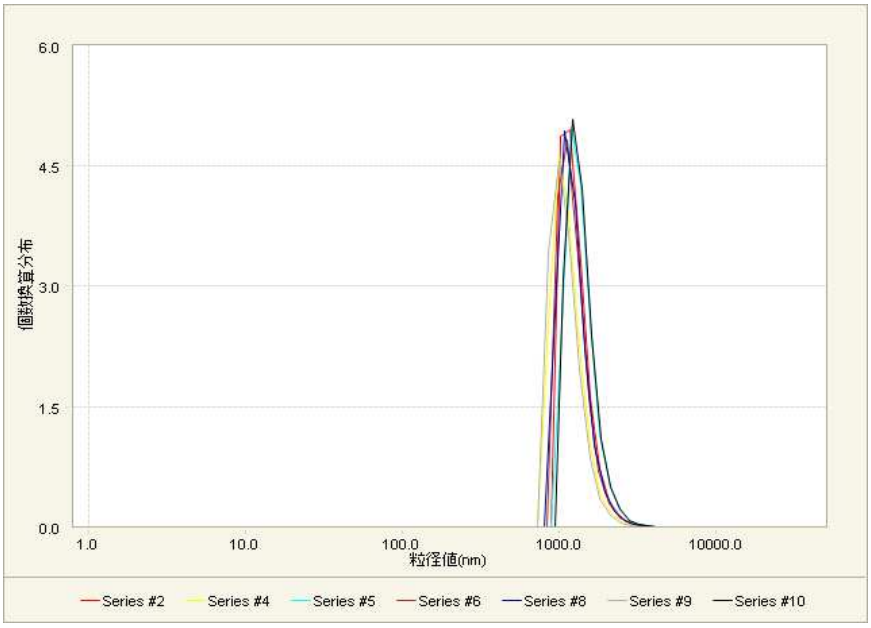

No.	DataName	Color	Diameter(nm)	Cumu.(10%)(nm)	Cumu.(50%)(nm)	Cumu.(90%)(nm)
1	20180118PFV-PSi-	Blue	513.2	119.9	254.6	340.2
2	20180118PFV-PSi-	Red	296.1	171.1	207.2	271.7
3	20180118PFV-PSi-	Green	266.3	127.1	156.3	212.6
4	20180118PFV-PSi-	Yellow	272	21.7	23.3	25.1
5	20180118PFV-PSi-	Cyan	258.5	102.6	130.8	182.6
6	20180118PFV-PSi-	Brown	265.7	33.1	35.6	38.4
7	20180118PFV-PSi-	Aqua	278.2	137.6	170.7	235.1
8	20180118PFV-PSi-	DarkBlue	287	139.1	169.7	229.2
9	20180118PFV-PSi-	DarkGray	281.5	125.3	157.8	219.2
10	20180118PFV-PSi-	Black	284.7	149.1	177.4	235.7

Figure S35. Changes in particle size of **PFV8-HPS-*R*** co-colloids in $CHCl_3$/MeOH = 2.0/1.0 (v/v) after the 313-nm UV irradiation (20 μW cm^{-2}) for 10 sec.

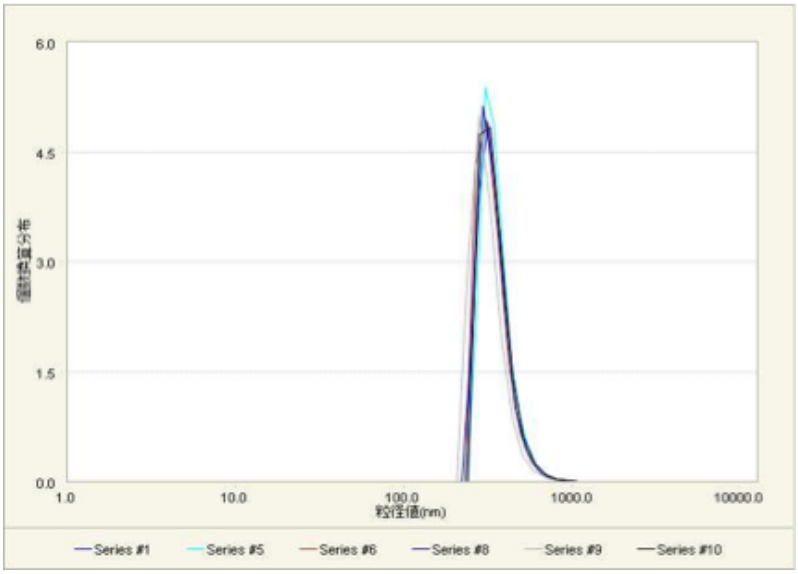

No.	DataName	Color	Diameter(nm)	Cumu.(10%)(nm)	Cumu.(50%)(nm)	Cumu.(90%)(nm)
1	20180118PFV-PSi-	Blue	734.5	249.0	307.6	423.4
2	20180118PFV-PSi-	Red	539.2	204.6	252.3	343.3
3	20180118PFV-PSi-	Green	558.3	341.4	418.1	556.8
4	20180118PFV-PSi-	Yellow	574	320.8	390.3	577.3
5	20180118PFV-PSi-	Cyan	592.4	267.2	320.3	431.2
6	20180118PFV-PSi-	Brown	612.7	245.3	299.2	407.6
7	20180118PFV-PSi-	Aqua	609	441.4	596.4	1029.2
8	20180118PFV-PSi-	DarkBlue	623	246.8	303.5	411.4
9	20180118PFV-PSi-	DarkGray	649.6	224.0	277.3	378.3
10	20180118PFV-PSi-	Black	654.2	255.1	309.1	422.0

Figure S36. Changes in in particle size of **PFV8-HCPS-*SR*** co-colloids [(*S*)/(*R*)= 0.50/0.50] in $CHCl_3$/MeOH = 2.0/1.0 (v/v) after the 313-nm UV irradiation (20 μW cm^{-2}) for 10 sec.

*4. Imaging co-colloidal **PFV8-HPS-S** by dynamic force modulation (DFM)-atomic force microscopy (AFM).*

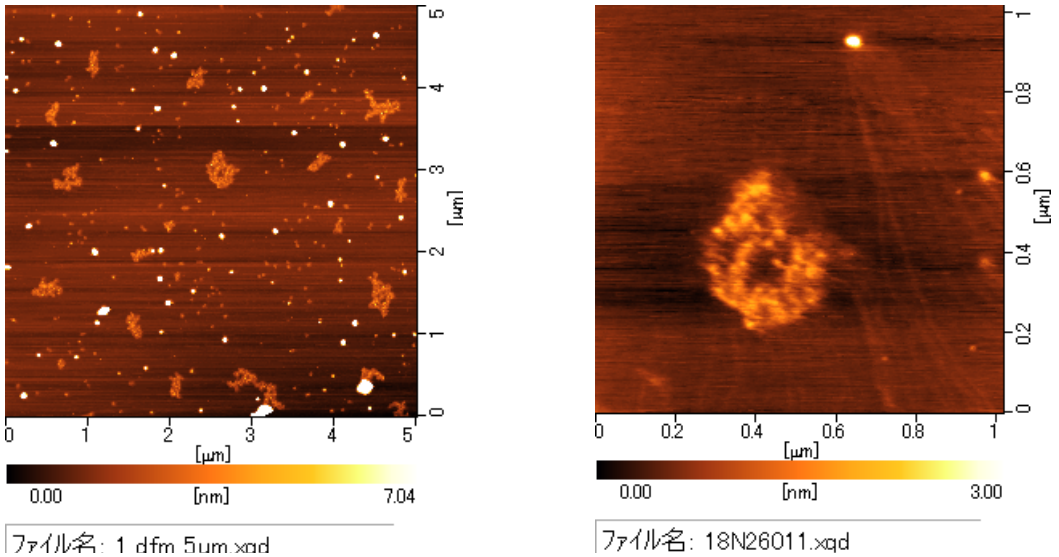

Figure S37. DFM-AFM images (left: raw image, right: its zoom-in image) of **PFV8-HPS-S** co-colloid (2:1 in mole ratio) in $CHCl_3$/MeOH = 2.0/1.0 (v/v) deposit on HOPG.

*5. Thin films from chirogenetic **PFV8** with **type I HCPS** and **PFV8** with **type II HCPS** onto glass substate.*

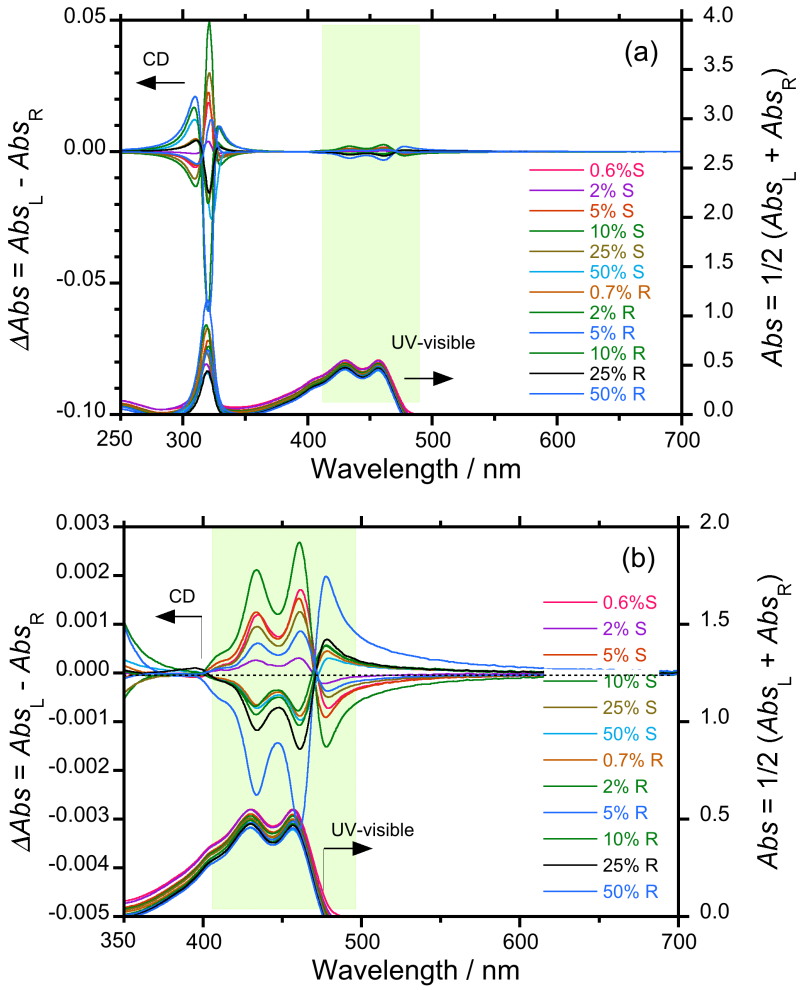

Figure S38. Sergeant-and-soldier in film state. Changes in CD spectra of **PFV8** with **type I HCPS** deposited onto Tempax glass substate.

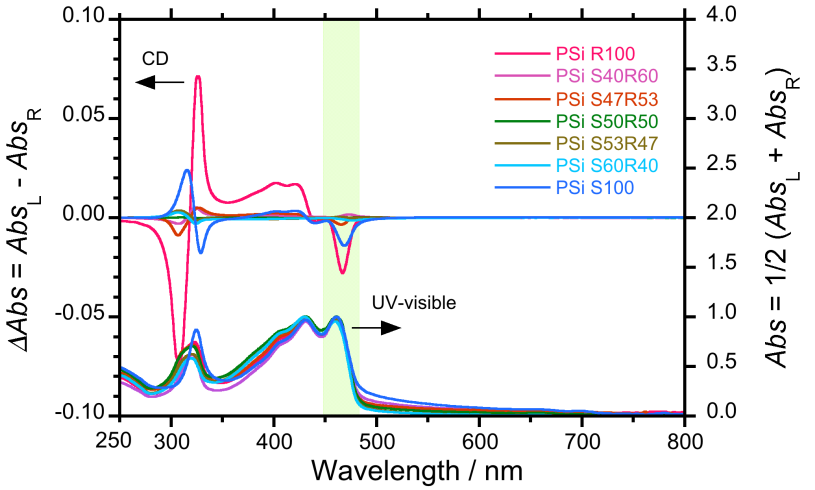

Figure S39. Majority rule in film state. Changes in CD spectra from **PFV8** with **type II HCPS** deposited onto Tempax Float® solid substate.

*6. Optimizing optofluidic effects of **PFV8** co-colloids with **HPS-S***

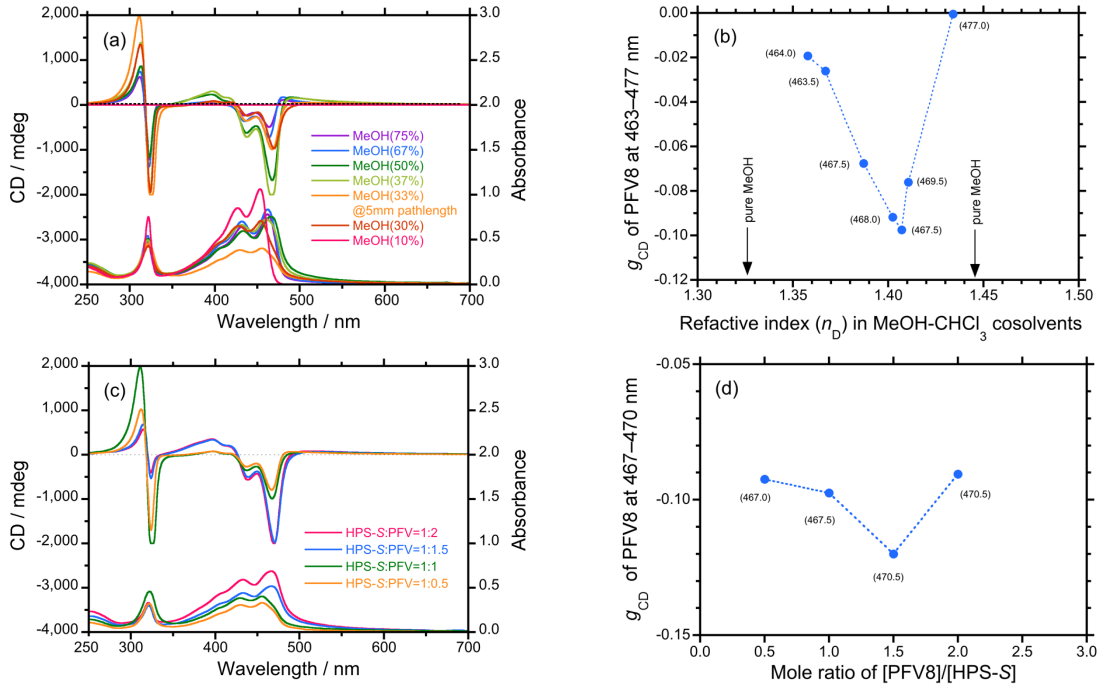

Figure S40. (a) The raw bisignate couplet-like CD and UV-visible spectra of co-colloids comprising **HPS-*S*** and **PFV8** (1:1 mole ratio) varying volume functions of MeOH in a series of $CHCl_3$/MeOH cosolvents. (b) The corresponding g_{CD} value of **PFV8** at the first Cotton band (λ_{ext}; 463.5–477.0 nm) as a function of refractive index (n_D). (c) The raw bisignate CD and UV-visible spectra of co-colloids at four different mol ratios of **PFV8**/**HPS-*S*** in $CHCl_3$/MeOH = 2.0/1.0 (v/v). (d) The g_{CD} value of **PFV8** at the first Cotton band (λ_{ext}; 467.0–470.5 nm) as a function of mole ratio of **PFV8**/**HPS-*S***.

In designing the controlled optofluidic co-colloidal systems including helical polysilane copolymers, **PFV8**, and a mixture of the surrounding poor-good co-solvents, we have to optimize the best mole ratios of **HPS-*S***, and **PFV8** and the best volume fraction in a mixture of the cosolvent enable to effectively confine light energy inside of the co-colloid. Because of the co-colloids are considerably swollen by the co-solvents, the RI value is a variable parameter. To maximize the optofluidic effects, we experimentally determined the best RI values of both the swollen co-colloids with a higher RI consisting of two polymers and the surrounding co-solvents with lower RI.

Figure S40(a) plots the changes in the raw bisignate CD and UV-visible spectra of co-colloids consisting of **HPS-*S*** and an equimolar amount as its repeating unit of **PFV8**, varying a volume fraction of MeOH (common poor solvent for **HPS-*S*** and **PFV8**) in a mixture of $CHCl_3$ and MeOH. $CHCl_3$ and MeOH are commonly good and poor solvents for **HPS-*S*** and **PFV8**, respectively. When a volume fraction of MeOH increases, the bisignate CD signals appear at ~320 nm due to **HPS-*S*** and the bisignate CD-visible spectra in the range of 350 nm and 480 nm due to π-π^* transitions of **PFV8** are obvious. Figure S40(b) plots the g_{CD} value at λ_{ext} (463.5–477.0 nm) of (–)-sign CD bands from **PFV8** in the colloids as a function of n_D of the cosolvents. The $|g_{CD}|$ value does not obey a monotonous increment with n_D value associated with volume fraction of MeOH. Clearly, the g_{CD} value boosts when $CHCl_3$/MeOH = 2.0/1.0 (v/v) at n_D = 1.407.

Next, to optimize a relative mole fraction of **PFV8** and **HPS** as their repeating units at the specific $CHCl_3$/MeOH = 2.0/1.0 (v/v), we obtained the similar bisignate CD and UV-visible spectra of **HPS-PFV8** co-colloids when a relative mole ratio of **PFV8** and **HPS** varies from 0.50 and 2.0, as shown in Figure S40(c). The 1.5/1.0 mole ratio of **PFV8** and **HPS** provides the greatest g_{CD} value at 465–467 nm of **PFV8**, as shown in Figure S40(d). The 1.5/1.0 mole ratio of **PFV8** and **HPS** exhibits slightly larger g_{CD} values compared to that at 1.0/1.0 and 2.0/1.0 mole ratios. Because of practical reason, we chose the 1.0/1.0 mole ratio of **PFV8** and **HPS** in the following experiments of **PFV8** co-colloids with **types I HCPS** and **II HCPS**.

7. Co-solvent dependency of ***PFV8*** *co-colloids with* ***HPS-S, -R****, and* ***type I HCPS***

7-1. In tetrahydrofuran (THF)/MeOH = 2/1 (v/v).

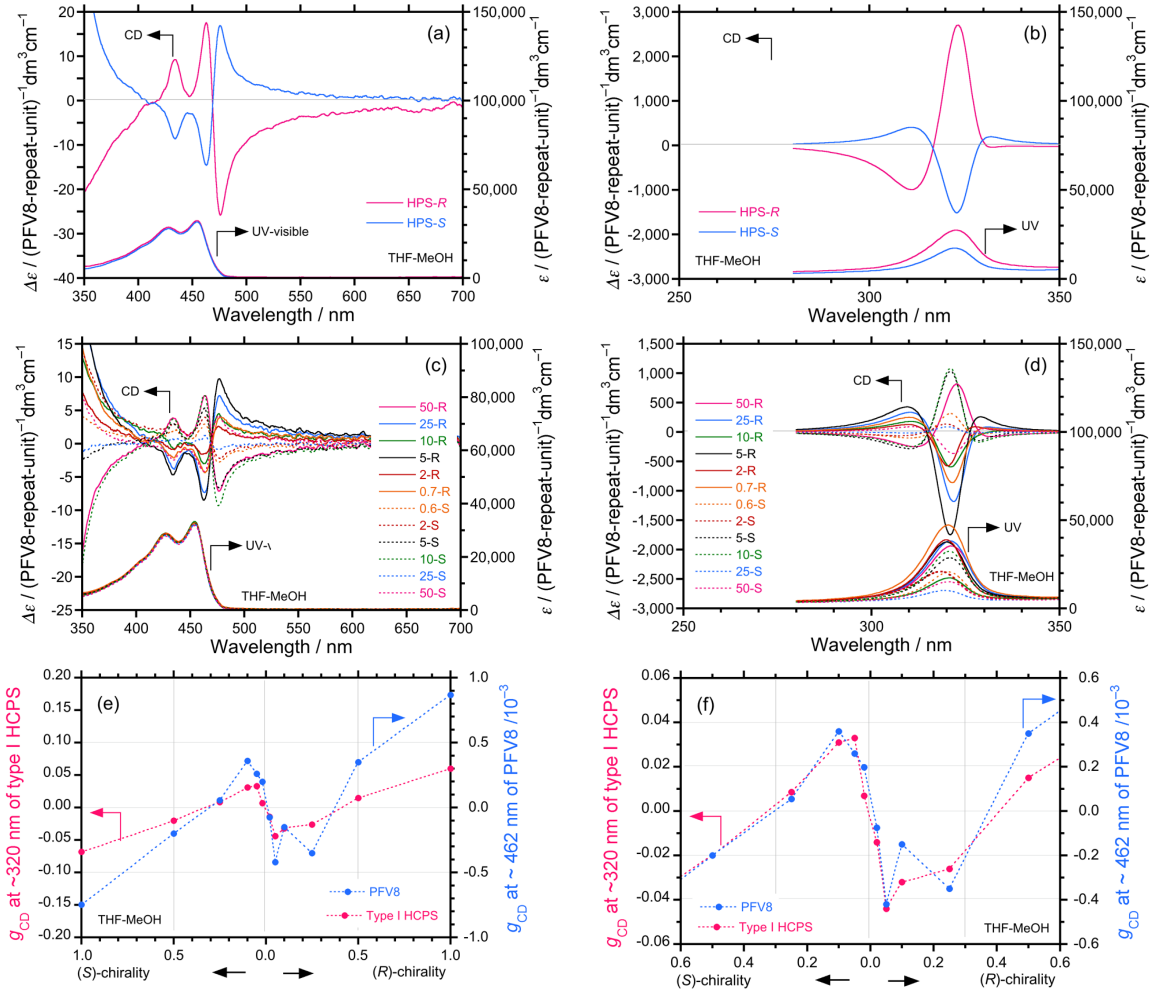

Figure S41. The raw bisignate couplet-like CD and UV-visible spectra of **PFV8** co-colloids with **HPS-*S*** and **-*R*** (1:1 mole ratio) and **type I HCPS-*S*** [(*S*) = 0.6, 2, 5, 10, 25, 50 mol %] and **-*R*** [(*R*) = 0.7, 2, 5, 10, 25, 50 mol %] (as 1:1 mole ratio) in THF/MeOH (2/1 (v/v)) cosolvents; (a) UV-visible region for **PFV8** with **HPS-*S*** and **-*R***, (b) UV region for **HPS-*S*** and **-*R*** with **PFV8**; (c) UV-visible region for **PFV8** with **type I HCPS-*S*** and **-*R***, and (d) UV region for **type I HCPS-*S*** and **-*R*** with **PFV8**. (e) The g_{CD} values of **PFV8** at ~ 462 nm (right ordinate, filled circles) and **HPS-*S***, **-*R***, **type I HCPS-*S***, and **-*R*** at ~ 320 nm (left ordinate, red circles) *vs.* mole fractions of the (*S*)-(*R*) and (f) its zoom-in plot.

7-2. In toluene/MeOH = 2/1 (v/v).

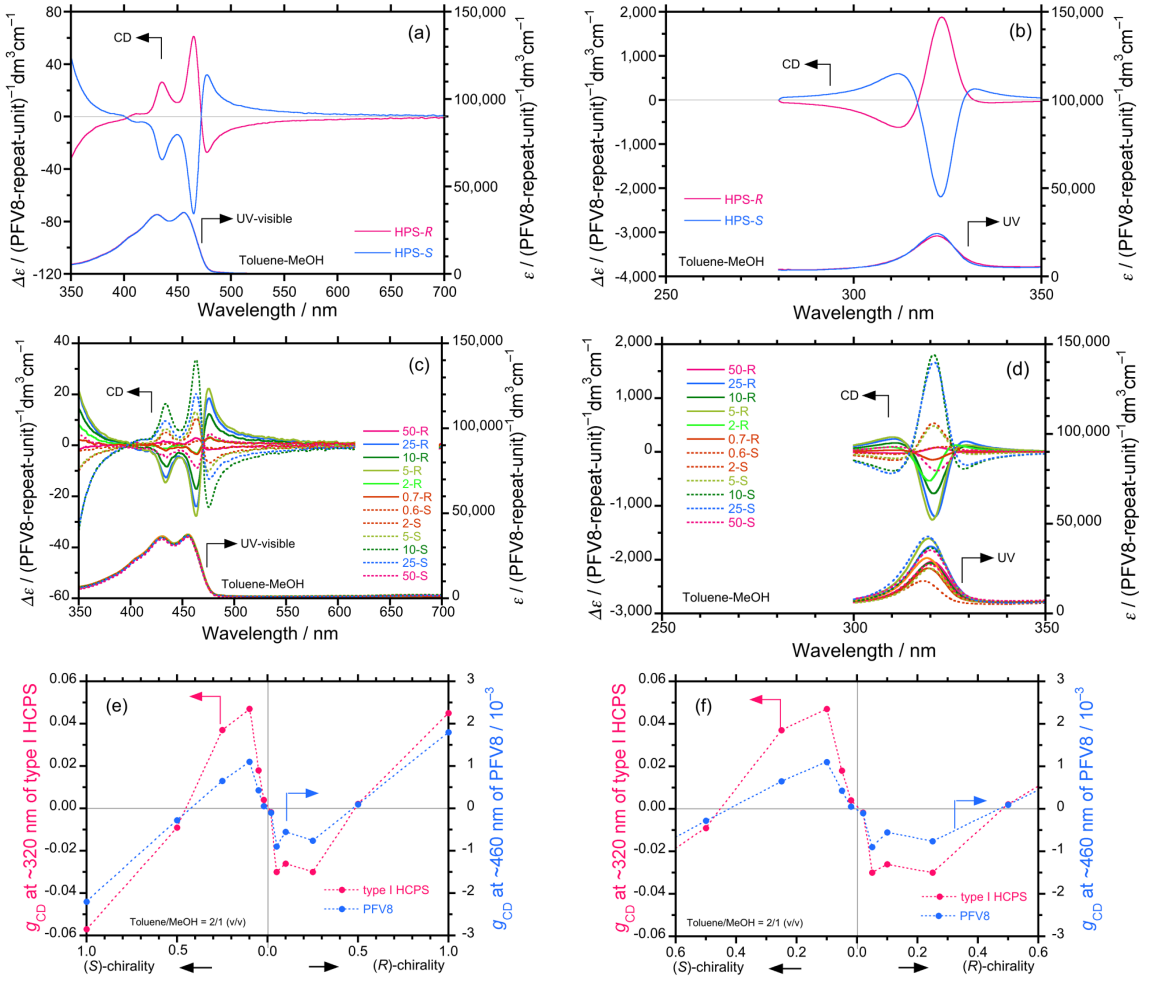

Figure S42. The raw bisignate couplet-like CD and UV-visible spectra of **PFV8** co-colloids with **HPS-*S*** and **-*R*** (1:1 mole ratio) and **type I HCPS-*S*** [(*S*) = 0.6, 2, 5, 10, 25, 50 mol %] and **-*R*** [(*R*) = 0.7, 2, 5, 10, 25, 50 mol %] (as 1:1 mole ratio) in toluene/MeOH (2/1 (v/v)) cosolvents; (a) UV-visible region for **PFV8** with **HPS-*S*** and **-*R***, (b) UV region for **HPS-*S*** and **-*R*** with **PFV8**; (c) UV-visible region for **PFV8** with **type I HCPS-*S*** and **-*R***, and (d) UV region for **type I HCPS-*S*** and **-*R*** with **PFV8**. (e) The g_{CD} values of **PFV8** at ~ 462 nm (right ordinate, filled circles) and **HPS-*S***, **-*R***, **type I HCPS-*S***, and **-*R*** at ~ 320 nm (left ordinate, red circles) *vs.* mole fractions of the (*S*)-(*R*) and (f) its zoom-in plot.

To maximize Ser-Sol effect of **PFV8** co-colloids with **HPS** and **type I HCPS**, we chose the best poor-good co-solvents fixed to 2/1 (v/v) that enable to effectively boost CD signals at π–π* transitions of **PFV8**.

Figure S41plots the raw bisignate couplet-like CD and UV-visible spectra of **PFV8** co-colloids with **HPS-*S*** and **-*R*** (1:1 mole ratio) in THF/MeOH (2/1 (v/v)) cosolvents; (a) UV-visible region of **PFV8** and (b) UV region for **HPS-*S*** and **-*R***. Also, the raw bisignate couplet-like CD and UV-visible spectra of **PFV8** co-colloids with **type I HCPS-*S*** [(*S*) = 0.6, 2, 5, 10, 25, 50 mol %] and **-*R*** [(*R*) = 0.7, 2, 5, 10, 25, 50 mol %] (1:1 mole ratio) in the cosolvents are given in (c) UV-visible region for **PFV8** and (d) UV region for **type I HCPS-*S*** and **-*R***. (e) The g_{CD} values at ~ 462 nm of **PFV8** (right ordinate, filled circles) and at ~ 320–324 nm of **type I HCPS-*S*** and **-*R*** (left ordinate, red circles) *vs.* mole fractions of the (*S*)-(*R*) and (f) its zoom-in plot are shown in Figure S41(e) and S41(f).

Figure S42 plots the raw bisignate couplet-like CD and UV-visible spectra of **PFV8** co-colloids with **HPS-*S*** and **-*R*** (1:1 mole ratio) in toluene/MeOH (2/1 (v/v)) cosolvents; (a) UV-visible region of **PFV8** and (b) UV region for **HPS-*S*** and **-*R***. Also, the raw bisignate couplet-like CD and UV-visible spectra of **PFV8** co-colloids with **type I HCPS-*S*** [(*S*) = 0.6, 2, 5, 10, 25, 50 mol %] and **-*R*** [(*R*) = 0.7, 2, 5, 10, 25, 50 mol %] (as 1:1 mole ratio) in the cosolvents in the cosolvents are displayed in; (c) UV-

visible region for **PFV8** and (d) UV region for **type I HCPS-*S*** and **-*R***. The g_{CD} values at ~ 462 nm of **PFV8** (right ordinate, filled circles) and at ~ 320–324 nm of **type I HCPS-*S*** and **-*R*** (left ordinate, red circles) *vs.* mole fractions of the (*S*)-(*R*) and its zoom-in plot are given in Figure S42(e) and S42(f).

By comparing the absolute value of g_{CD} values at ~ 460 nm of **PFV8** in three good–poor cosolvents ($CHCl_3$-MeOH (Figure 4 in the main text), THF-MeOH, and toluene-MeOH) are in the order of $CHCl_3$-MeOH ($|g_{CD}|$ = (50 – 100) x 10^{-3}) >> toluene-MeOH [$|g_{CD}|$ = ~2 x 10^{-3}] > THF-MeOH [$|g_{CD}|$ = (0.6 – 0.9) x 10^{-3}]. Noted that chiroptical inversion between 25 mol % and 50 mol % of (*S*)-(*R*) pendant chirality occurs commonly regardless of the three cosolvents.

2. References

S1. Rahim, N.A.A.; Fujiki, M. Aggregation-induced Scaffolding: Photoscissable Helical Polysilane Generates Circularly Polarized Luminescent Polyfluorene. *Polym. Chem*. **2016**, *7*, 4618-4629.

S2. Takamizu, K.; Inagaki, A.; Nomura, K. Precise Synthesis of Poly(fluorene vinylene)s Capped with Chromophores: Efficient Fluorescent Polymers Modified by Conjugation Length and End-Groups. *ACS Macro Lett.* **2013**, *2*, 980–984.

S3. Fujiki, M.; Yoshida, K.; Suzuki, N.; Zhang, J.; Zhang, W.; Zhu, X. Mirror Symmetry Breaking and Restoration within μm-Sized Polymer Particles in Optofluidic Media by Pumping Circularly Polarised Light. *RSC Adv.* **2013**, *3*, 5213–5219.

S4. Fujiki, M.; Donguri, Y.; Zhao, Y.; Nakao, A.; Suzuki, N.; Yoshida, K.; Zhang, W. Photon Magic: Chiroptical Polarisation, Depolarisation, Inversion, Retention and Switching of Non-Photochromic Light-Emitting Polymers in Optofluidic Medium. *Polym. Chem*. **2015**, *6*, 1627-1638.

S5. Duong, S.T.; Fujiki, M. The Origin of Bisignate Circularly Polarized Luminescence (CPL) Spectra from Chiral Polymer Aggregates and Molecular Camphor: Anti-Kasha's Rule Revealed by CPL Excitation (CPLE) Spectra. *Polym. Chem*. **2017**, *8*, 4673-4679.

S6. Fujiki; M.; Yoshimoto, S. Time-evolved, Far-red, Circularly Polarised Luminescent Polymer Aggregates Endowed with Sacrificial Helical Si–Si Bond Polymers. *Mater. Chem. Front.*, **2017**, *1*, 1773-1785.